The Roles of Hydroxyl Radicals and Superoxide in Oxidizing Aqueous Benzyl Alcohol under Ultrasound Irradiation.

Ari F. Fischer[1,2], Teseer Bahry[3], Zhangyue Xie[1], Roberto Batista da Silva Junior[4], Kaicheng Qian[5], Renhong Li[5], James Kwan[6], François Jerome[3], Sabine Valange[3,4], Wen Liu[1,2], Prince N. Amaniampong[3,4]* and Tej S. Choksi[1,2]*

[1]*School of Chemistry, Chemical Engineering and Biotechnology, 62 Nanyang Drive, Nanyang Technological University, 637459, Singapore, Singapore.*

[2]*Cambridge Centre for Advanced Research and Education in Singapore (CARES), 1 Create Way, 138602, Singapore, Singapore.*

[3]*CNRS, Université de Poitiers, Institut de Chimie des Milieux et Matériaux de Poitiers, 1 rue Marcel Doré, Bat B1 (ENSI-Poitiers), 86073 Poitiers, France*

[4]*CNRS@CREATE Ltd., 1 Create Way, #15-01, CREATE Tower, Singapore, 138602, Singapore*

[5]*National Engineering Lab for Textile Fiber Materials and Processing Technology, Zhejiang Sci-Tech University, Hangzhou, 310018, China*

[6]*Department of Engineering Science, University of Oxford, Parks Road, Oxford OX1 3PJ, United Kingdom*

Keywords: advanced oxidation • sonochemistry • conjugate addition • DFT • wastewater treatment • radical chain reactions

Abstract

The abatement of aromatic pollutants in water requires resource-intensive oxidation to nontoxic products by hydroxyl radicals (•OH). In this study, we elucidate the mechanisms of •OH-induced aromatic ring degradation by combining kinetic measurements, electron paramagnetic resonance spectroscopy, density functional theory (DFT) calculations, and kinetic modelling. We demonstrate that benzyl alcohol, a model aromatic compound, is oxidized by •OH radicals, generated by ultrasonic irradiation in an O_2-rich environment, into aromatic compounds (benzaldehyde and phenol derivatives) and C1-C2 oxygenates (formic acid, glyoxal, and oxalic acid). Through pathways akin to atmospheric chemistry, these •OH radicals de-aromatize and fragment benzyl alcohol, producing 5-hydroxy-4-oxo-pentenal and other dicarbonyl products. Unique to the aqueous phase, however, superoxide ($•O_2^-$) is generated as a byproduct of •OH-benzyl alcohol reactions. $•O_2^-$ acts as a potent nucleophile, oxidizing 5-hydroxy-4-oxo-pentenal into oxalic acid and C1 oxygenates via aldehyde and ketone intermediates. This process regenerates $•O_2^-$ and does not consume •OH, thereby further degrading ring fragmentation products while preserving •OH to activate the refractory aromatic ring of benzyl alcohol. These nucleophilic $•O_2^-$ reactions can therefore reduce the energy and chemical demands needed to degrade aromatic compounds, thus promoting the sustainable and scalable application of •OH-based oxidation processes in water treatment.

Table of contents graphic

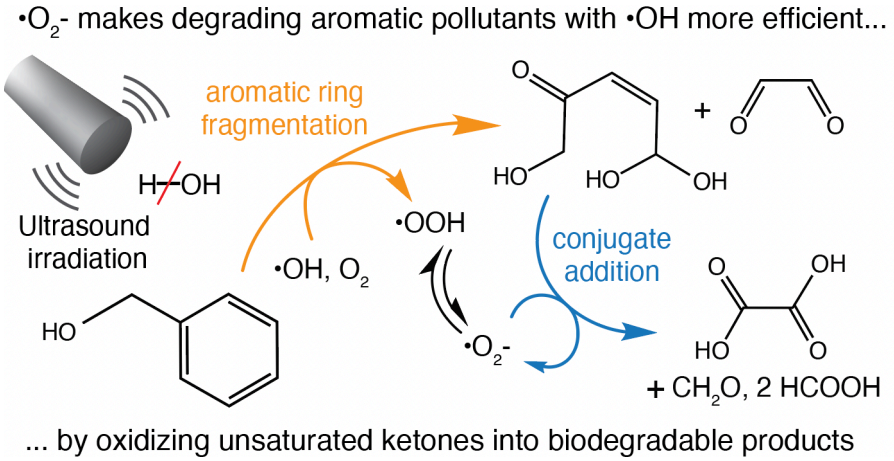

1. Introduction

Benzene and its derivatives (e.g., phenylacetic acid, ibuprofen) are contaminants of municipal[1–4], industrial[5,6], and agricultural[2] wastewaters. The adverse consequences of these aromatic compounds for human and ecological health[3,7] necessitates their removal from wastewater streams before discharge or reuse. Aromatic compounds resist oxidation by biochemical processes [8,9] and chemical oxidants[8–10] (e.g., ozone, chlorine, hypochlorite) typically used in wastewater treatment. They can however be degraded by hydroxyl radicals (•OH), which are generated in advanced oxidation processes[11] by dissociating H_2O_2 with ultraviolet radiation[10–12] or with Fenton reactions[11,13], or by dissociating H_2O in gas cavities using ultrasound irradiation[14–18].

Advanced oxidation processes incur substantial operational costs from chemical inputs (e.g., H_2O_2) and energy required to generate •OH from H_2O or sacrificial reagents[19–22]. A mechanistic understanding of aromatic ring oxidation by •OH can inform strategies to reduce the quantities of •OH needed to degrade aromatic compounds into biodegradable products[10,21,23]. Aqueous aromatic compounds (e.g., benzene[24,25] and toluene[26]) are oxidized by •OH through ring cleavage into biodegradable short-chain dicarbonyl products (e.g. glyoxal[24,26], methylglyoxal[26]) and carboxylic acid products (e.g. formic acid[24,26] and acetic acid[26]). These fragmentations are proposed to occur through mechanisms[24,26] (**Scheme 1**) that resemble those established in gas-phase chemistry[27–33]. Gas-phase benzene fragmentation, for instance, begins with •OH addition to the aromatic ring, followed by reaction with O_2 to form a bicyclic peroxyl radical intermediate (**step 1**, **Scheme 1**). The bicyclic peroxyl radical undergoes a chain of radical reaction steps that cleaves two C-C bonds, yielding one stoichiometric equivalent of glyoxal (a α-carbonyl-aldehyde) and butenedial (a γ-carbonyl-alk-2-enal) or its epoxide (**step 2, Scheme 1**)[28]. Substituted benzene derivatives (e.g., toluene and benzyl alcohol) convert into analogs of the benzene-derived fragments, with the substituent replacing one of the C-H groups (**Scheme 1**).

Scheme 1: Steps for de-aromatization and fragmentation of a "X"-substituted benzene derivative. These fragmentations form a set of isomeric products with the X-function located at either R_1, R_2, and R_3 positions. The location of X in the products depends on its initial ring location relative to the location where •OH adds to the phenyl ring, and to the points of C-C cleavage. A comprehensive sequence of elementary steps for such fragmentation and an enumeration of different isomers formed are shown for benzyl alcohol (X=CH_2OH) in **Figures 3** and **S1**, respectively.

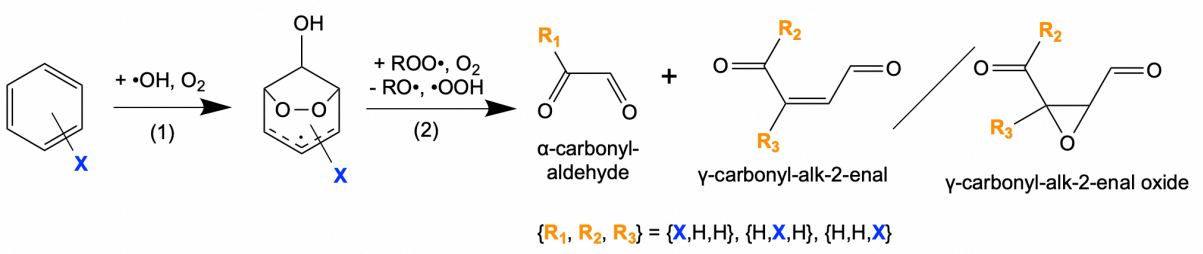

In contrast with the fragmentation of aromatic compounds in the gas phase[27–33], organic acids (e.g., formic acid[24,26] and acetic acid[26]) are formed as primary products during the fragmentation of aromatic compounds in the aqueous phase. This difference in selectivity to organic acids between aqueous- and gas-phase reactions suggests that solvation by water influences the mechanisms of fragmentation in the aqueous phase[26]. Intermediates formed during •OH-initiated aromatic fragmentation react with O_2 via hydrogen transfer, generating hydroperoxyl radicals (•OOH) as a by-product[27,28,31]. In aqueous solutions, •OOH equilibrates with its conjugate base, superoxide ($•O_2^-$)[34,35]. $•O_2^-$ has been reported to react as a nucleophile in substitution[36,37], addition[37], and elimination[37] reactions in aprotic solvents, and in addition reactions to the aldehyde function of glyoxal in aqueous solution[38]. Tts nucleophilicity suggests that it can attack the electrophilic α-β unsaturated carbonyl functions of γ-carbonyl-alk-2-enals. Such an attack by $•O_2^-$ could facilitate further oxidation of γ-carbonyl-alk-2-enals to organic acids without requiring additional •OH initiators.

In this study, we combine computational and experimental techniques to investigate the mechanisms of aqueous •OH-initiated aromatic ring fragmentation in an O_2 environment, and the role of $•O_2^-$ therein at a pH near the point of •OOH/$•O_2^-$ equilibration (4.62 at 315 K [34]). Benzyl alcohol (5 mM) is used because it undergoes alcohol oxidation, aromatic substitution, and ring fragmentation

reactions[28–30], making it an ideal model of aromatic compounds with diverse functional groups. The •OH is generated by ultrasound irradiation (20 kHz), but the mechanistic insights are agnostic to the source of •OH.

Experimental measurements of benzyl alcohol oxidation rates and density functional theory (DFT)-based kinetic modeling show that •OH-initiated reactions fragment benzyl alcohol into 5-hydroxy-4-oxo-pentenal and glyoxal through established mechanisms of gas-phase chemistry[27–33], echoing proposals for other aromatic compounds[24,26]. These experimental and computational kinetic investigations indicate that the 5-hydroxy-4-oxo-pentenal product of fragmentation is activated by $•O_2^-$ through conjugate addition to the α-β unsaturated carbonyl function. The adduct undergoes a radical-chain reaction that forms oxalic acid with molar yields that exceed 0.25 of the benzyl alcohol consumed. Such reactions between $•O_2^-$ and 5-hydroxy-4-oxo-pentenal are infeasible in the gas-phase, which lacks the protic solvent needed for $•O_2^-$ charge stabilization. Consequently, the reactions propagated by $•O_2^-$ account for the large yields of oxalic acid from •OH-initiated benzyl alcohol oxidation in aqueous phase, despite oxalic acid not being reported as a product from analogous reactions in the gas-phase[28]. $•O_2^-$ is prevalent in •OH-driven oxidations of diverse organic substrates reactions of hydrated aldehydes[39–41], alcohols[41,42], organic acids[41,43], and arenes[24,26], suggesting a broader role of the types of $•O_2^-$ reactions with carbonyl functions reported here in water treatment. Such $•O_2^-$ reactions oxidize organic molecules with carbonyl functions without depleting •OH initiators, thereby preserving •OH to activate refractory organic molecules. Harnessing $•O_2^-$ as an oxidant can therefore reduce the costs of generating •OH in advanced oxidation processes for treating municipal, industrial, and agricultural wastewaters.

2. Results and discussion

2.1. Ultrasound-derived hydroxyl radicals drive the consumption of benzyl alcohol and formation of aromatic compounds

Aqueous benzyl alcohol oxidation by ultrasound irradiation was carried out in a double-jacketed batch reactor with continuous exposure to ultrasound waves (20 kHz; 0.27 W cm^{-3} at 50% amplitude) and bubbling O_2 (1 atm, 0.33 cm^3 s^{-1}; **Section S1.1**). **Figure 1** shows the change in benzyl alcohol concentration with time of ultrasound irradiation (5 mM initial benzyl alcohol; 315 K). The

benzyl alcohol concentration decreased linearly with time, reflecting a constant rate of consumption (1.7×10^{-8} M s^{-1}; **Fig. 1**). The consumption of benzyl alcohol was slower than the characteristic rate that •OH was supplied to the aqueous solution by ultrasound-driven cavitation processes (2.6×10^{-8} M s^{-1}), as reported using the same reactor in our previous study[38]. This characteristic rate was quantified by titrating the H_2O_2 product of •OH coupling reactions in the absence of an organic substrate[44]. The relatively faster rate of •OH formation (2.6×10^{-8} M OH s^{-1}) indicates that the supply of •OH is stoichiometrically sufficient to initiate the oxidation pathways of benzyl alcohol (at 1.7×10^{-8} M s^{-1}).

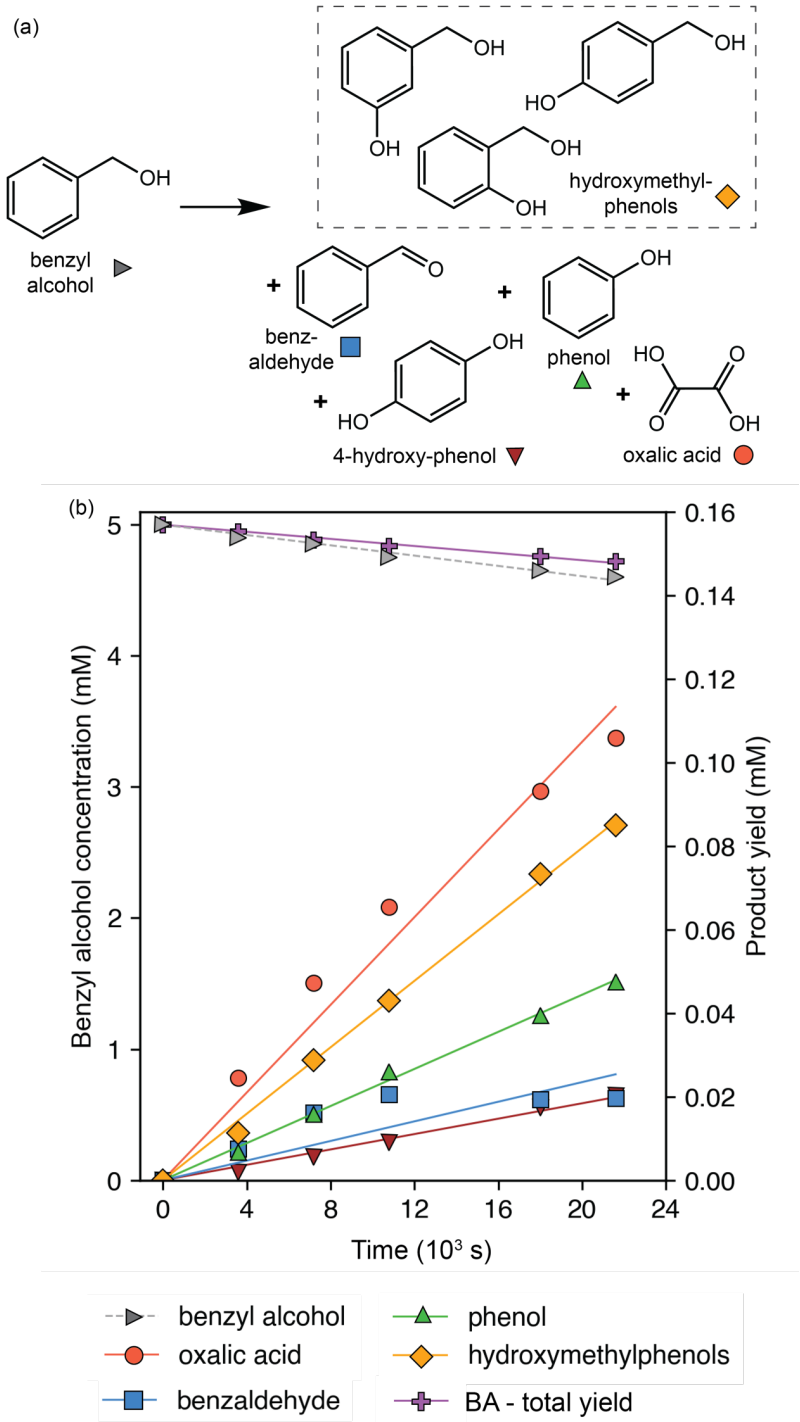

Figure 1. (a) Schematic depicting benzyl alcohol conversion to products quantified from sonochemical benzyl alcohol oxidation (**Section S1.1**). (b) The change in aqueous benzyl alcohol concentration and product yields with time of exposure to continuous ultrasonic irradiation under bubbling O_2 (5 mM benzyl alcohol; 20 kHz; 315 K; **Section S1.1**). The purple "+" represents the benzyl alcohol concentration with the total yield of quantified products subtracted (denoted as "BA - total yield"). The solid and dashed lines depict fits of linear functions. Initial rates were calculated from the slope of a linear trendline with zero intercept regressed to measurements collected within 1.1×10^4 s (**Table S16**).

Electron paramagnetic resonance (EPR) spectra were collected from sonicated mixtures of aqueous 5,5-dimethyl-1-pyrroline N-oxide (DMPO; 50 mM) and benzyl alcohol (0-50 mM), to assess whether •OH-benzyl alcohol reactions are fast enough to compete with rapid •OH-addition to DMPO. The spectra were collected following exposure to pulsed ultrasound irradiation (3 s on, 1 s off) at 20 kHz for 1.2×10^3 s under flow of O_2 (**Section S1.2**); these spectra are shown in **Figure 2**. The spectra of 0- and 5-mM benzyl alcohol solutions showed a predominant feature consistent with an adduct formed by •OH addition to DMPO (denoted as DMPO/OH). This DMPO/OH signal was relatively weaker at 5 mM benzyl alcohol, and essentially undetectable at 25 and 50 mM benzyl alcohol. Such suppression of the DMPO/OH signal with increasing benzyl alcohol concentration suggests that •OH is scavenged by benzyl alcohol in the aqueous phase thus preventing the •OH addition to DMPO. This rapid nature of •OH-benzyl alcohol reactions, combined with commensurate rates of •OH formation (2.6×10^{-8} M s^{-1} [38]) and benzyl alcohol consumption (1.7×10^{-8} M s^{-1}; **Fig. 1**), suggests that aqueous •OH-initiated reactions are the predominant drivers of benzyl alcohol consumption during the kinetic studies of benzyl alcohol oxidation shown in **Figure 1**.

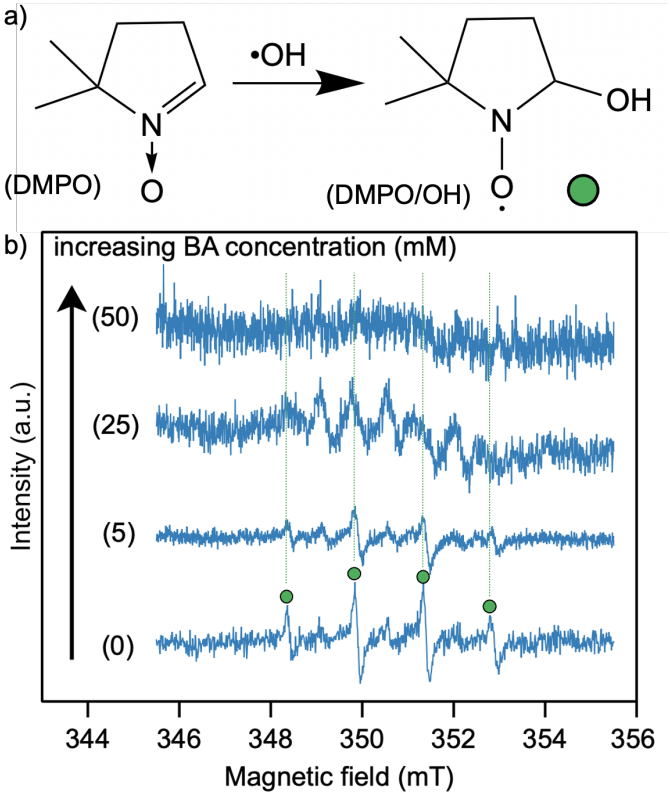

Figure 2. (a) Scheme depicting •OH addition to 5,5-dimethyl-1-pyrroline N-oxide (DMPO) to form the DMPO-•OH adduct (DMPO/OH). (b) Electron paramagnetic resonance (EPR) spectra for aqueous solutions of 5,5-dimethyl-1-pyrroline N-oxide (DMPO; 50 mM) mixed with benzyl alcohol (BA) at different concentrations (0-50 mM) following exposure to pulsed ultrasound irradiation at 20 kHz under flow of O_2 (0.33 cm^3 s^{-1}) for 1.2 $\times 10^3$ s (**Section S1.2)**. The magnetic field values corresponding to peak values for the DMPO/OH single are denoted by the green circle. One and five scans were used to collect the spectra for solutions with 0 and 5 mM BA and 25 and 50 mM BA, respectively.

The benzyl alcohol-•OH reactions sustained under ultrasound irradiation formed aromatic compounds including benzaldehyde, phenol, 4-hydroxy-phenol, and hydroxymethyl-phenol isomers. The yields of each aromatic product were between 0.020 mM and 0.047 mM after 2.2×10^4 s (**Table S17**). The combined yield to these aromatic compounds after 2.2×10^4 s (0.17 mM) balanced a significant fraction (0.47) of the benzyl alcohol consumed (0.36 mM; **Fig. 1**). The remaining fraction (0.53) of benzyl alcohol consumed (0.19 mM) was thus converted into other products.

The other products include oxalic acid, which was formed at a yield (0.11 mM) that balanced nearly one-third (0.29) of the benzyl alcohol consumed after 2.2×10^4 s (0.36 mM; **Fig. 1**). The short linear carbon chain in oxalic acid (2 C-atoms) compared to larger cyclic C-backbone of benzyl alcohol (7 C-atoms) indicates that oxalic acid formation from benzyl alcohol would require ring opening and fragmentation. The plausible mechanisms for such routes from benzyl alcohol to oxalic acid are examined in **Sections 2.2** and **2.3**.

Benzaldehyde, phenol, hydroxymethyl-phenol isomers, and hydroxy-phenol isomers were reported as products from the gas-phase oxidation of benzyl alcohol in the presence of O_2 and initiated by •OH, which was generated by CH_3ONO photolysis[30,45]. A proposed sequence of elementary steps for the formation of benzaldehyde, phenol, hydroxymethyl-phenol isomers was adapted from mechanistic studies of reactions in the gas-phase[28,30,45] and shown in **Scheme 2**. The mechanisms for forming 4-hydroxy-phenol were not considered because its initial rate of formation (within the first 1.2×10^4 s) was smaller than for the other aromatic compounds (**Table S16**).

Steps 1a-2a (**Scheme 2**) show H-transfer from benzyl alcohol to •OH (**step 1a**) to form hydroxy-(phenyl)methyl•, which further reacts via hydroxy H-transfer to O_2 to form benzaldehyde and •OOH (**Step 2a**). **Steps 1b-2b** show •OH addition to benzyl alcohol at the C1 position to form 6-hydroxymethyl-6-hydroxy-cyclohexadienyl• (denoted as *ipso*-BA/•OH; **step 1b**), followed by hydroxymethyl• elimination to form phenol (**step 2b**). **Steps 1c** shows •OH addition to benzyl alcohol at the C2, C3, or C4 positions to form 2-, 3-, or 4-hydroxymethyl-6-hydroxy-cyclohexadienyl•, respectively (denoted as *ortho-, meta-,* or *para*-BA/•OH, respectively). In **step 2c**, these cyclohexadienyl• intermediates undergo H-transfer with O_2 to form •OOH and hydroxymethyl phenol isomers. These isomers include 2-hydroxymethyl-phenol, the predominant isomer from gas-phase reactions[28,30,45], and 3- and 4-hydroxymethyl phenol isomers which were detected alongside 2-hydroxymethyl-phenol in sonochemical reactions (**Fig. 1**).

The reactions in **Scheme 2** also show that •OOH forms as a by-product through H-abstraction by O_2. Unlike in the gas-phase, •OOH deprotonates to $\bullet O_2^-$ through an acid-base equilibrium in aqueous solutions. Such $\bullet O_2^-$ species are nucleophiles and will mediate the formation of oxalic acid, as will be discussed in **Section 2.3**.

Scheme 2 also shows the changes in Gibbs free energy (ΔG) and forward rate constants (315 K) for each elementary reaction at reaction temperature (315 K; **Fig. 1**), as calculated using density-functional theory (DFT) methods (**Section S2.1-2**). The DFT calculations were performed with QChem[46], using a range-separated hybrid, meta-GGA functional (ωB97M-V[47]) and with solute interactions with the H_2O solvent introduced implicitly using the SMD model[48] (**Section S2.1**). Rate constants were determined using transition-state theory[49,50] and accounted for resistance to reaction from diffusion[51,52] (**Section S2.2**). The forward rate constants computed using DFT methods for •OH-addition to benzyl alcohol (1.3 to 2.8 $\times 10^9$ M^{-1} s^{-1}; **Scheme 2, steps 1b,c**) are comparable to those reported from kinetic analysis of •OH-benzyl alcohol reactions using pulsed radiolysis (8.4 $\times 10^9$ M^{-1} s^{-1})[53].

The rate constants for •OH-addition reactions (**steps 1b** and **1c**; **Scheme 1**) were within a factor of 3 of each other (1.1 to 2.5 $\times 10^{-9}$ M^{-1} s^{-1}; **Scheme 2**), reflecting the competitive nature of •OH addition at all locations in the ring. This observation contrasts reports in the gas phase where •OH adds preferentially to the C1 and C2 positions due to H-bonding between the -OH function of benzyl alcohol with the •OH moiety at the transition states for these reactions[28]. The relatively less selective •OH addition at the C1 and C2 positions in the aqueous phase likely reflects the stabilizing interactions between the •OH dipole and the implicit solvent at transition states corresponding to all of these •OH addition reactions. These interactions with the solvent diminish the influence of H-bonding between •OH and the hydroxymethyl group of benzyl alcohol that would otherwise favor •OH addition to the C1 and C2 positions.

The rate constants for benzyl alcohol-•OH reactions ($k_{i,OH,BA}$; **Scheme 2, steps 1a,b,c**) were within 20-fold of the rate constant for diffusive encounters (k_d; **Table S11**) between freely diffusing •OH and either •OH, benzyl alcohol, or prevalent oxidation products (**Fig. 1**). Each k_d value (1.1-2.3$\times 10^{10}$ M^{-1} s^{-1}; **Table S11**) represents the maximum possible rate that •OH can react with a given co-reactant, assuming instantaneous reaction upon contact in solution. The large rate constants for benzyl alcohol-•OH reactions, near their diffusion limits, aligns with interpretations of EPR measurements (**Fig. 2**), which indicated that •OH was rapidly scavenged by benzyl alcohol, thereby preventing •OH addition to DMPO. The oxidation studies (**Fig. 1**) were conducted with excess benzyl alcohol (>4.7 mM benzyl

alcohol; **Fig. 1)** compared to the lower concentrations of predominant products (< 0.11 mM oxalic acid, < 0.05 mM aromatic compounds; **Fig. 1**). The large values of $k_{i,OH,BA}$ indicate that rates of •OH-benzyl alcohol reactions far exceed the rates of •OH reactions with other solutes, even when diffusion-limited, during kinetic measurements (**Fig. 1**). Consequently, benzyl alcohol effectively scavenges all •OH initiators.

The reactive nature of free radicals[54] suggests that the radicals intermediates in **Scheme 2** react instantaneously once formed to establish low pseudo-steady state concentrations. A pseudo-steady-state approximation for these radical intermediates is justified as long as pseudo-first-order rate constants for their consumption are much larger than those for their formation from benzyl alcohol[55]. This justification, based on rate constants, stems from perturbation treatments of kinetic models of chemical reactions[56].

The pseudo-first-order rate constant for benzyl alcohol consumption under ultrasonic irradiation (3.8×10^{-6} s^{-1}) was obtained by dividing the initial measured consumption rate (1.9×10^{-8} M s^{-1}; **Table S16**) by the initial benzyl alcohol concentration (5 mM). This rate constant was 10^6-times smaller than the DFT-derived first-order rate constant calculated for hydroxymethyl• elimination from *ipso*-BA/•OH (1.2 s^{-1}; **step 2b**; **Scheme 2**). It was also 10^8-times smaller than the DFT-derived pseudo-first-order rate constants for the reactions of hydroxy-(phenyl)-methyl• and the other benzyl alcohol-•OH adducts with O_2 (**step 2a** and **2c**; **Scheme 2**; at 0.99 mM O_2 present in equilibrium with 1 bar O_2 gas). The larger calculated (pseudo-) first-order rate constants for reactions of hydroxy-(phenyl)-methyl• and benzyl alcohol-•OH adducts, compared to the measured pseudo-first-order rate constant for benzyl alcohol consumption, confirms the pseudo-steady-state nature of these radical intermediates[55,56].

The occurrence of the benzyl alcohol substitution and alcohol oxidation reactions in **Scheme 2** at pseudo-steady state indicates that benzaldehyde, phenol, and hydroxymethyl-phenol isomers form essentially instantaneously once benzyl alcohol is activated by •OH. The pseudo-steady-state nature of these reactions, taken together with the measured rate of •OH formation (2.6×10^{-8} M s^{-1} [38]) being sufficient to drive measured rates of benzyl alcohol consumption (1.9×10^{-8} M s^{-1}; **Table S16**), suggests that the predominant aromatic products form via •OH-initiated reactions of benzyl alcohol.

Scheme 2: Sequence of elementary steps for the •OH-initiated conversion of benzyl alcohol to benzaldehyde (1a,2a), phenol (1b,2b), and ortho, meta, and para hydroxymethyl phenol isomers (1c,2c). Square brackets show forward rate constants (k_i (M^{n-1} s^{-1}, with *n* number of reactants); **Section S2.2**) and braces show reaction free energies ({ΔG}) evaluated with DFT-based methods (315 K, **Section S2.1**). The values in (1c and 2c) show ranges of values for steps that form different hydroxymethyl phenol isomers.

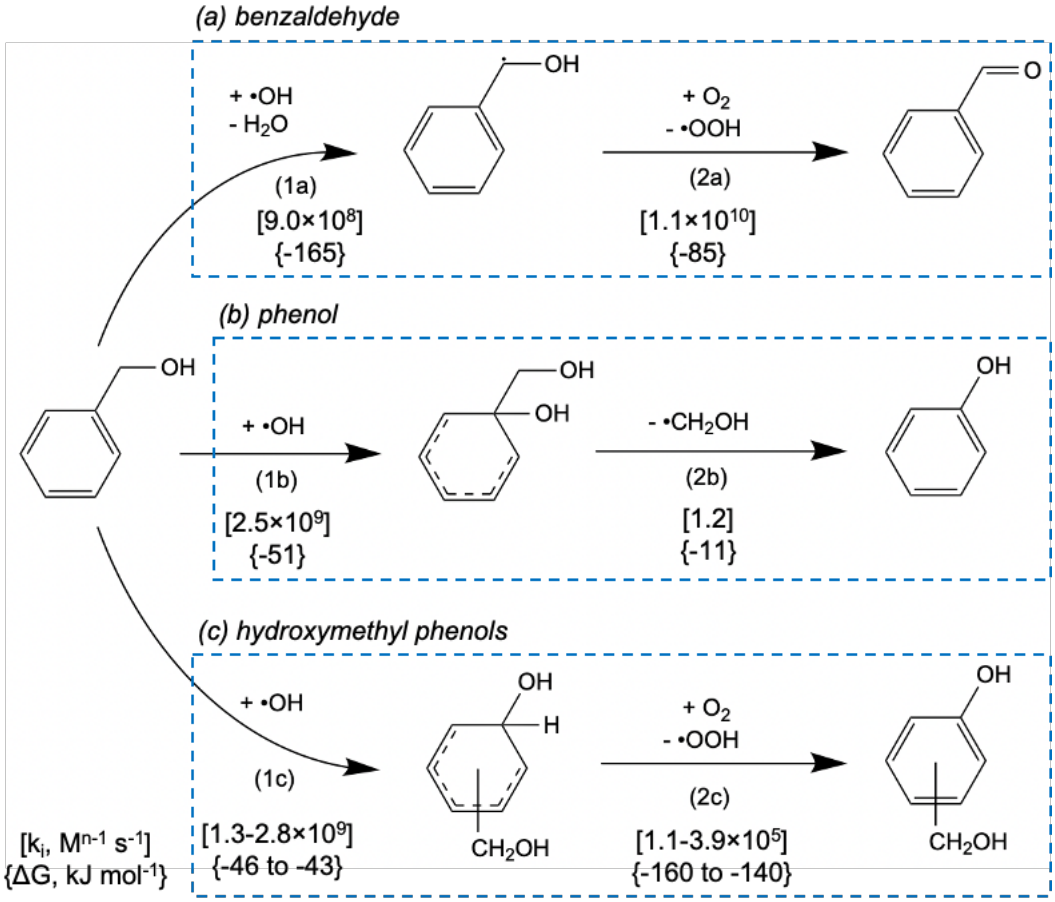

2.2. Benzyl alcohol-•OH adducts mediate aromatic ring fragmentation into dicarbonyl products. The •OH-benzyl alcohol adducts, formed as intermediates in pathways to phenol and hydroxymethyl phenol isomers (**steps 1b-2b** and **1c-2c**; **Scheme 2**), can also react with O_2 through addition to their rings. The addition of O_2 to •OH adducts of various aromatic compounds has been implicated in pathways for fragmenting aromatic compounds into dicarbonyl products in the gas-phase[27,28,31–33,45,57–

[59]. The fragmentation of benzyl alcohol through such mechanisms yields one stoichiometric equivalent of an α-carbonyl-aldehyde (i.e., glyoxal or 3-hydroxy-2-oxopropanal) and a γ-carbonyl-alk-2-enal (i.e., but-2-enedial, 2-hydroxymethyl-but-2-enedial, or 5-hydroxy-4-oxo-pent-2-enal) or the epoxide form of the γ-carbonyl-alk-2-enal[28]. The specific product pair depends on the locations of the •OH and O_2 additions to the benzyl alcohol ring relative to the hydroxymethyl function, as shown in **Scheme S1**.

A calculation of the average oxidation state for C-atoms in oxalic acid based on formal charges gives a value of 3, which is closer to that for carbonyl-aldehyde fragmentation products (0 for δ-carbonyl-alk-2-enals and 0.4 to 0.5 for their epoxides) than for benzyl alcohol (-0.86). This comparison between oxidation states implies that the conversion of fragmentation products to oxalic acid requires fewer further oxidation reactions than the conversion of benzyl alcohol to oxalic acid. These carbonyl-aldehyde intermediates therefore constitute plausible intermediates in pathways that form oxalic acid from benzyl alcohol reactants when exposed to ultrasonic irradiation, provided that the mechanisms that form them in the gas-phase[27,28,31–33,45,57–59] are also prevalent in the aqueous phase.

Scheme 3: Reactions of benzyl alcohol-•OH adducts that initiate ring fragmentation (2a-5a) or form substitution products (2b-5b), and the forward rate constants calculated for each step (k_i (M^{n-1} s^{-1}, with *n* number of reactants) at 315 K; **Section S2**).

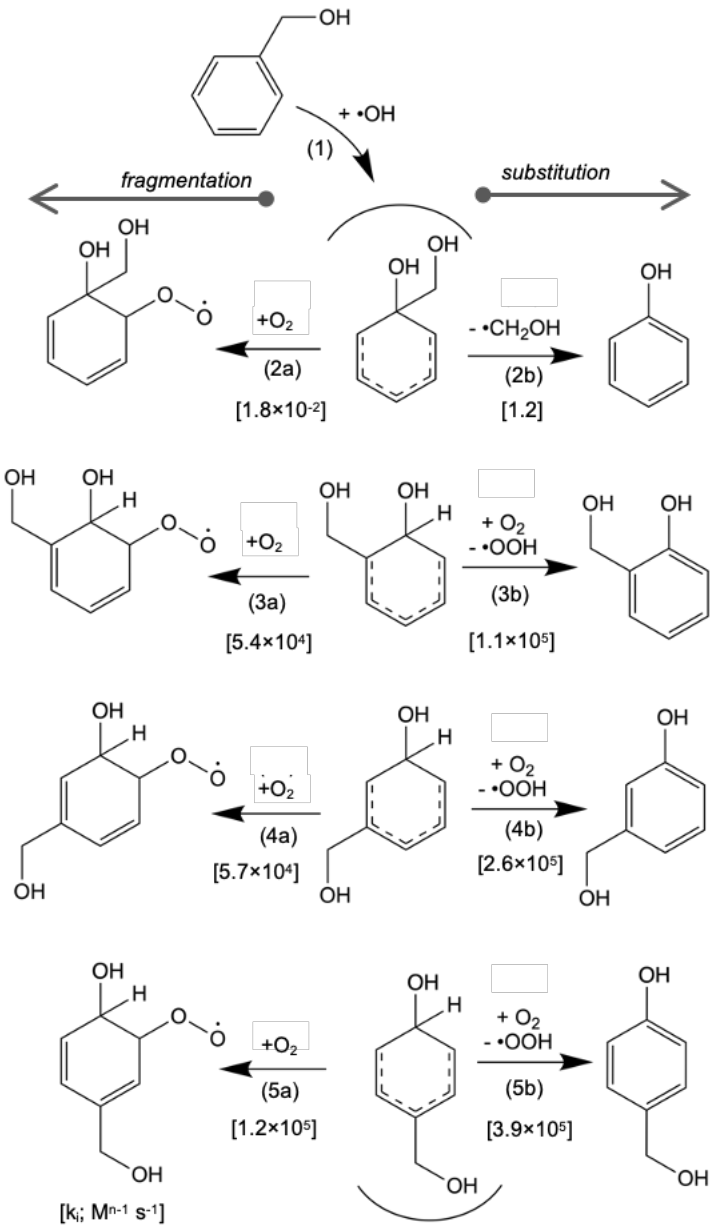

The fragmentation of benzyl alcohol-•OH adducts is mediated by peroxyl radicals formed through O_2 addition to the ring at vicinal locations to the -OH function[27,28,59]. **Scheme 3** shows such O_2 additions to *ipso*-, *ortho*-, *meta*-, and *para*-BA/•OH (**steps 2a-5a**) and their rate constants calculated with DFT-based methods (**Section S2**). O_2 additions to *ortho*-, *meta*-, and *para*-BA/•OH (**steps 3a-5a**) are shown to occur at the a*nti*-position (i.e., with O_2 adding to the ring opposite to the -OH function) instead of the *syn*-position (i.e., with O_2 adding to the same side of the ring as the -OH function). This reflects the preference for *anti*-O_2 addition to •OH adducts of aromatic compounds, which is evident from a lower free energy barrier calculated for *anti*-O_2 addition to benzene ($\Delta G^{\ddagger}$; 47 kJ mol^{-1}) than for *syn*-O_2 addition (73 kJ mol^{-1}; **Section S3**). **Steps 3a** and **4a** show O_2 addition to *ortho*- and *meta*-

BA/•OH at the 5 positions, instead of the 1 position, to minimize steric hindrance from the hydroxymethyl function. O_2 addition to *ipso*-BA/•OH (**step 2a**) is shown with -OO and -OH functions in the *syn*-conformation, reflecting the lower barrier to form this conformer compared with the *anti*-counterpart[28].

Scheme 3 also shows the substitution reactions of these same benzyl alcohol-•OH adducts (**steps 2b-5b**) and their forward rate constants. The rate constant calculated for O_2 addition to *ipso*-BA/•OH (**step 2a**) is 67 times smaller than that of unimolecular hydroxymethyl• elimination (**step 2b**); therefore, O_2 addition occurs at rates that are negligible at O_2 concentrations prevalent under sonochemical conditions (0.99 mM O_2 in equilibrium with flowing O_2 at 1 bar[60]). The forward rate constants for O_2 addition to *ortho-, meta-*, and *para*-BA/•OH (**steps 3a-5a**), in contrast, were 2, 5, and 3 times smaller, respectively, than rate constants for H-transfer reactions of these same adducts (**steps 3b-5b**). The similar magnitude of rate constants for these O_2 addition and H-transfer reactions with *ortho-, meta-*, and *para*-BA/•OH reflects significant competition between these pathways.

DFT-based methods with implicit H_2O solvation (described in **Sections S2**) were used to assess whether the adducts formed by O_2 addition to BA/•OH intermediates fragment in the aqueous phase through the same mechanisms that prevail in the gas-phase[28]. Fragmentation through the *ortho*-BA/•OH intermediate was considered because it has the largest ratio between rate constants for O_2 addition and H-transfer among the •OH adducts (**Scheme 3**), and therefore most likely to fragment. The sequence of elementary steps for *ortho*-BA/•OH fragmentation to glyoxal and 5-hydroxy-4-oxo-pentenal is shown in **Figure 3**, along with the free energy changes (ΔG) and free energy barriers ($\Delta G^{\ddagger}$) for each step. The overall reaction occurs with a large negative free energy change (-529 kJ mol^{-1}), reflecting a significant thermodynamic driving force.

Steps 1-4 (**Fig. 3b**) show the conversion of benzyl alcohol, •OH, and 2 O_2 into a bicyclic radical intermediate (denoted as bicyclo(*ortho*-BA)-OO•; **Fig. 3b**), which consists of a peroxyl radical functionalized by an allylic cyclohexyl moiety with a -CH_2OH function at the 4 position, -OH function at the 5 position, and a peroxide group bridging the 4 and 6 positions (denoted as bicyclo(*ortho*-BA)-; **Fig. 3b**). **Steps 1** and **2** (**Fig. 3b**) shows sequential •OH and O_2 addition to benzyl alcohol through the same reactions shown in **Scheme 1** (**step 2c**) and **Scheme 2** (**step 3b**), respectively. Such sequential

additions yield 5-hydroxymethyl-6-hydroxy-cyclohexa-2,4-dienyl-peroxyl•. This peroxyl• intermediate reacts further (**step 3; Fig. 3b**) by intramolecular peroxyl attack at the 5-position of the cyclohexadienyl function, forming bicyclo(*ortho*-BA)•. Bicyclo(*ortho*-BA)• further reacts in **step 4** (**Fig. 3b**) through O_2 addition at the allyl group to form bicyclo(*ortho*-BA)-OO• (**Fig. 3b**).

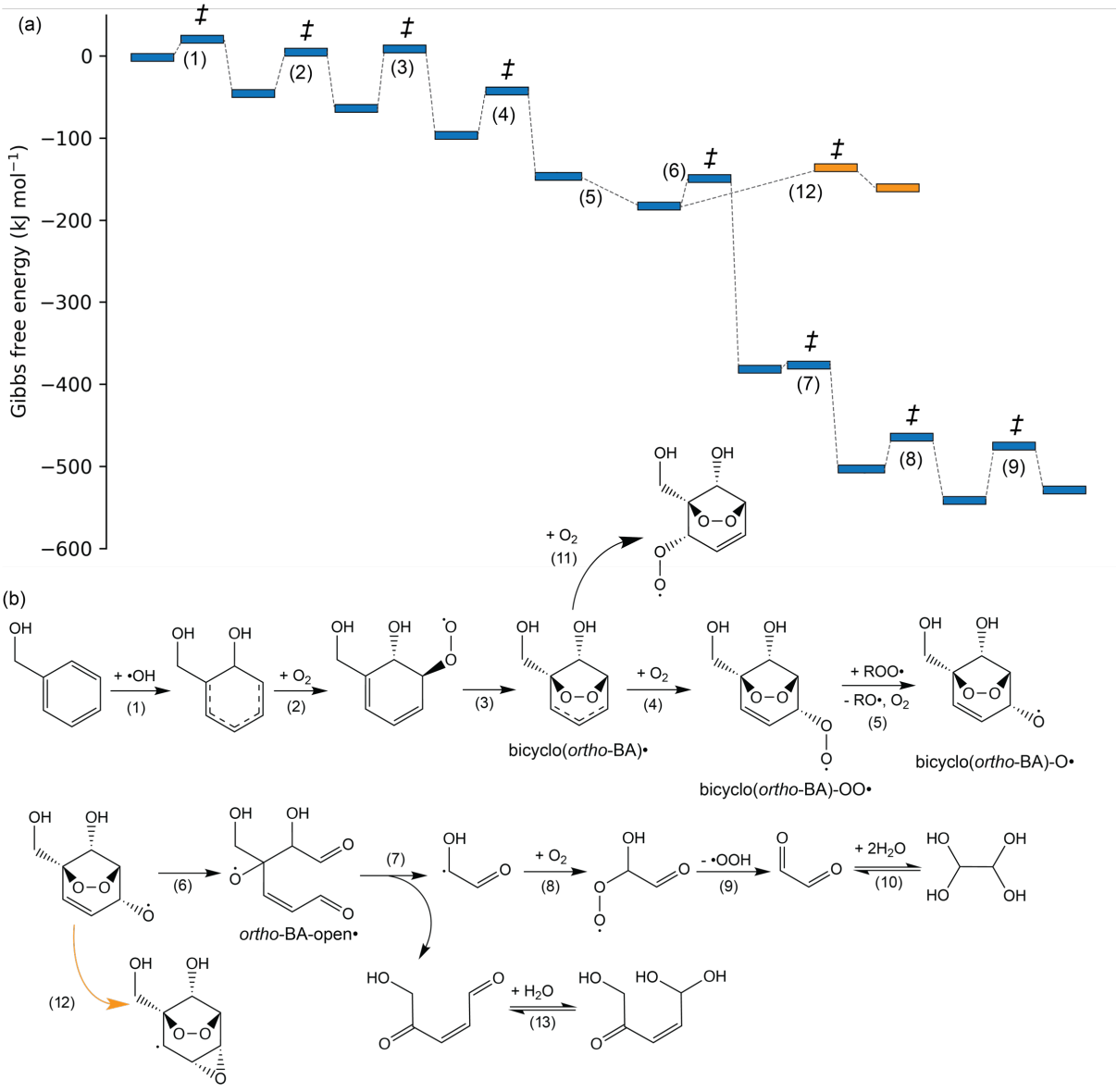

Figure 3: (a) The Gibbs free energies (315 K) of intermediates and transition states (denoted with ‡) for the fragmentation of benzyl alcohol through reaction steps in (b), calculated using DFT-based methods (**Section S2.1**). (b) Sequence of elementary steps for the fragmentation of benzyl alcohol to hydrated 5-hydroxy-4-oxo-pentenal and glyoxal in the presence of O_2 initiated by •OH addition to the α carbon.

Steps 5-11 (**Fig. 3b**) show the ring opening and fragmentation of bicyclo(*ortho*-BA)-OO• to form 5-hydroxy-4-oxo-pentenal, glyoxal, and •OOH. **Step 5** shows a bimolecular reaction between bicyclo(*ortho*-BA)-OO• and another peroxyl radical (ROO•), eliminating O_2 and forming two alkoxyl• products (bicyclo(*ortho*-BA)-O• (**Fig. 3b**) and RO•). Such oxygen transfer reactions of secondary peroxyl radicals (e.g., cyclohexylperoxyl•, cyclopentylperoxyl•, hydroxycyclohexylperoxyl•) occur in aqueous phase with rapid rate constants of order 10^7 to 10^8 M^{-1} s^{-1}[54,61]. **Step 6** shows the ring-opening of bicyclo(*ortho*-BA)-O• into an alkoxyl radical functionalized by a 6-oxo-5-hydroxy-4-hydroxymethyl-hex-2-enal moiety (denoted as *ortho*-BA-open•; **Fig. 3b**). This step involves the opening of both cyclohexenyl and dioxolanyl rings via concerted C-C and O-O cleavage. In **step 7**, *ortho*-BA-open• undergoes β-cleavage to form 5-hydroxy-4-oxo-pentenal and 2-oxo-1-hydroxyl-ethyl•. 2-oxo-1-hydroxyl-ethyl• reacts further by adding O_2 to form 2-oxo-1-hydroxyl-ethylperoxyl• (**step 8**). The 2-oxo-1-hydroxyl-ethylperoxyl• undergoes •OOH elimination to form glyoxal (**step 9**). **Steps 10** and **12** show the hydration of aldehyde functions in glyoxal and 5-hydroxy-4-oxo-pentenal products.

Glyoxal exists predominantly in its di-hydrated form (denoted as glyoxal.$2H_2O$) in aqueous solution[62]. The equilibrium for the hydration of 5-hydroxy-4-oxo-pentenal also likely favors the hydrated form (denoted as 5-hydroxy-4-oxo-pentenal.H_2O), given the presence of butenedial, which has an analogous unsaturated alkene-al group, is present predominantly as a hydrate[63]. These observations motivated us to consider hydrated forms of these aldehydes when investigating their further oxidation in **Section 2.3**. However, DFT calculations of these aldehyde hydration reactions show that, in contrast with experimental reports, the aldehyde form is thermodynamically favored (**Table S9**).

The bicyclo(*ortho*-BA)-O• intermediate can also undergo epoxidation by intramolecular O• attack of the vicinal C=C bond[28] (**step 7**; **Fig. 3**). The cyclic epoxide formed in **step 7** can also fragment, producing glyoxal and 5-hydroxy-4-oxo-pentenal epoxide[28]. The calculated $\Delta G^{\ddagger}$ value for the bicyclo(*ortho*-BA)-O• epoxidation reaction (44 kJ mol^{-1}) was 13 kJ mol^{-1} larger than the $\Delta G^{\ddagger}$ value for ring opening (**Fig. 3**); this relatively larger barrier indicates that bicyclo(*ortho*-BA)-O• epoxidation occurs negligibly during benzyl alcohol fragmentation. Such relatively slow bicyclo(*ortho*-BA)-O• epoxidation in the aqueous phase contrasts reports in the gas-phase where such oxyl• intermediates undergo epoxidation and ring-opening at comparable rates[28].

The addition of O_2 to bicyclo(*ortho*-BA)• is shown in **step 4** (**Fig. 3b**) to occur at the 1 position of the allyl group, instead of the 3 position. The free energy barrier for O_2 addition at the 1 position (54 kJ mol^{-1}) is only slightly lower than O_2 addition at the 3 position (55 kJ mol^{-1}), however, suggesting that bicyclo(*ortho*-BA)• reacts through both routes competitively. The O_2 addition at the 3-position forms a peroxyl• intermediate that ultimately fragments into 3-hydroxy-2-oxo-propanal and butenedial products (**step 2b**; **Scheme S1**), instead of the glyoxal and 5-hydroxy-4-oxo-pentenal products formed from fragmentation of bicyclo(*ortho*-BA)-OO•. Such competition between O_2 additions at different locations in the allyl group, together with the possible fragmentation of *meta*- and *para*-BA/•OH to glyoxal and 2-hydroxymethyl-but-2-enedial (**steps 2e** and **2f**; **Scheme S1**), suggests that benzyl alcohol fragmentation would likely form 3-hydroxy-2-oxo-propanal, butenedial, and 2-hydroxymethyl-but-2-enedial alongside the glyoxal and 5-hydroxy-4-oxo-pentenal products formed in **Figure 3b**.

The reactive nature of free radicals[54] suggests that the *ortho*-BA/•OH fragmentation reactions (**Fig. 3b**) occur rapidly at pseudo-steady state. This is supported by comparing the calculated rate constants for these reactions (**Fig. 3b**) with the measured rates of benzyl alcohol consumption (1.9×10^{-8} M s^{-1}; **Table S16**), as discussed in **Section S6**. The pseudo-steady-state nature of the reactions in **Figure 3b** indicates that they occur almost instantaneously upon benzyl alcohol activation by •OH (**steps 1**; **Fig. 3b**), making them plausible pathways for benzyl alcohol consumption under the supply of •OH from ultrasound-induced cavitation processes. Benzyl alcohol fragmentation through this *ortho*-BA/•OH fragmentation route is consistent with the detection of glyoxal, a primary fragmentation product (**Fig. 3b**), in the product solution of benzyl alcohol oxidation analyzed with high-performance liquid chromatography (HPLC). The glyoxal yields were not quantified, however, because the signals from glyoxal overlapped with other features in the HPLC chromatographs.

The fragmentation of benzene in the aqueous phase via the same •OH-initiated process for ortho-benzyl alcohol fragmentation was examined using DFT methods in **Section S4**. The changes in free energies for each elementary step in benzene fragmentation (**Table S8**) differed by less than 20 kJ mol^{-1} from those in ortho-benzyl alcohol fragmentation (**Table S9**), with free energy barriers differing by no more than 10 kJ mol^{-1} in magnitude. These comparable changes in free energy and free energy barriers suggests that benzene fragmentation is also feasible, and indicates, more broadly, that aqueous

benzene and its substituted derivatives undergo similar fragmentation processes, as observed in the gas-phase[27–33].

2.3. Superoxide mediates 5-hydroxy-4-oxo-pentenal conversion to oxalic acid.

Converting benzyl-alcohol-fragmentation products (i.e., glyoxal.2H_2O or 5-hydroxy-4-oxo-pentenal.H_2O) into oxalic acid requires activation by oxidants other than •OH. This is because •OH is scavenged by nearly diffusion-limited reactions with excess amounts of benzyl alcohol present during sonochemical reactions (**Section 2.1**). The •OH-benzyl alcohol reactions that form aromatic products (**Scheme 2**) and fragmentation products (**Fig. 3b**) also form •OOH. •OOH exists in equilibrium with its conjugate base, $•O_2^-$ in aqueous solution[35,64,65]. The nucleophilicity of $•O_2^-$ suggests it could initiate oxidation to oxalic acid by attacking the electrophilic α-β unsaturated carbonyl function of 5-hydroxy-4-oxo-pentenal.H_2O. The activation of glyoxal.2H_2O or 5-hydroxy-4-oxo-pentenal.H_2O by •OOH and peroxyl• intermediates were also considered but were found to occur at rates that were too slow to be relevant to oxalic acid formation, as discussed in **Section S8**.

Scheme 4 shows a mechanism proposed to convert 5-hydroxy-4-oxo-pentenal.H_2O into oxalic acid through a sequence of steps initiated by $•O_2^-$. The three remaining C-atoms form two formic acid molecules and formaldehyde. **Steps 1** and **2** show elementary reactions while **steps 3**, **4**, and **5** group multiple elementary steps together. A comprehensive sequence of elementary steps for these reactions is shown in **Scheme S3** (21 elementary steps in total). This mechanistic proposal is consistent with the detection of formic acid in the products of benzyl alcohol oxidation analyzed with HPLC. The yields of formic acid were not quantified, however, because the signals from formic acid overlapped with other features in the HPLC chromatographs.

Step 1 in **Scheme 4** shows conjugate $•O_2^-$ addition to 5-hydroxy-4-oxo-pentenal.H_2O, with $•O_2^-$ added to the β C-atom (relative to the carbonyl). This addition forms a peroxyl radical functionalized by a pentenolate moiety (1,5,5-trihydroxy-2-oxy-pent-2-en-4-yl), denoted as 5-hydroxy-4-oxo-pentenal.H_2O/$•O_2^-$ (**Scheme 4**). **Step 2** (**Scheme 4**) shows proton transfer from H^+ to 5-hydroxy-4-oxo-pentenal.H_2O/$•O_2^-$ at the α-position relative to the peroxyl group. This proton transfer forms a peroxyl• intermediate functionalized by a 1,5,5-trihydroxy-2-oxo-pentan-4-yl moiety (1,5,5-trihydroxy-2-oxo-

pentan-4-yl-peroxyl•). Such protonation is shown to occur at the carbanion to form the relatively stable keto tautomer[66] in favor of the enol tautomer. The weak acidity of α-carbons in ketones suggests that 5-hydroxy-4-oxo-pentenal.H_2O/•O_2^- protonates irreversibly (**step 2**).

Scheme 4: Sequence of steps proposed for •O_2^--initiated oxidation of hydrated 5-hydroxy-4-oxo-pentenal to oxalic acid, formic acid, and formaldehyde in the presence of O_2. Changes in free energies (ΔG; 315 K) for each step were calculated with DFT methods (**Section S2.1**). The blue underlines identify species molecules with closed valence shells. Single arrows denote elementary reactions and double arrows denote groups of sequential reactions. The detailed elementary steps that comprise steps 3, 4, and 5 are shown **Scheme S3**.

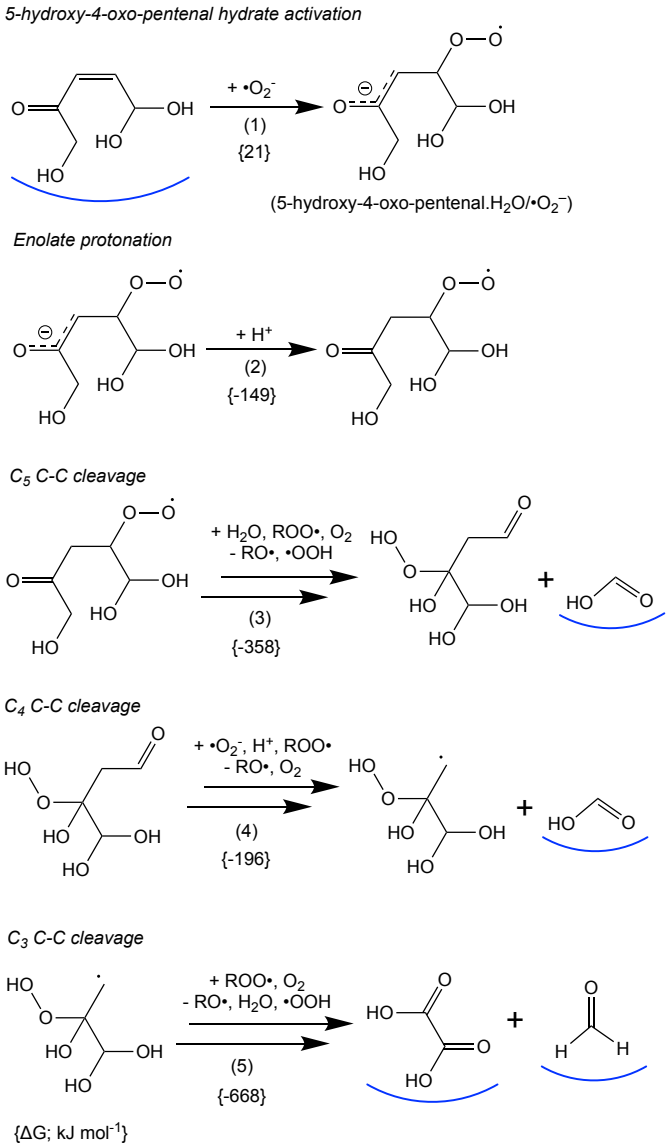

Steps 3-5 (**Scheme 4**) show a series of C-C cleavage reactions that convert 1,5,5-trihydroxy-2-oxo-pentan-4-yl-peroxyl• into two formic acid molecules (**steps 3** and **4**), oxalic acid (**steps 5**), and formaldehyde (**steps 5**). **Step 3** converts the 5-carbon peroxyl• intermediate formed in **step 2** into 3-hydroperoxy-3,4,4-trihydroxybutanal and formic acid as organic products. **Step 4** (**Scheme 4**) converts the butanal product of **Step 3** into 2-hydroperoxy-2,3,3-trihydroxypropyl• and formic acid. This sequence is initiated by $•O_2^-$ adding to the aldehyde function of 3-hydroperoxy-3,4,4-trihydroxybutanal (**step 12**; **Scheme S2**). **Step 5** (**Scheme 4**) converts the 2-hydroperoxy-2,3,3-trihydroxypropyl• intermediate into oxalic acid and formaldehyde. **Steps 3** and **5** both yield •OOH which, upon deprotonation, regenerates the $•O_2^-$ and H^+ reactants involved in **Steps 1**, **2**, and **4**. The 5-hydroxy-4-oxo-pentenal.H_2O oxidation reactions in **Scheme 4** consequently propagate the chain of radical reactions initiated by •OH, without terminating radical intermediates.

DFT-based methods with implicit H_2O solvation (described in **Sections S2**) were used to calculate the free energies of reaction, free energy barriers, and rate constants for the steps in **Scheme 4** and elementary steps that mediate them (**Scheme S3**; **Table S10**) at reaction temperature (315 K). The free energy changes for the steps in **Scheme 4** are reported therein. **Step 1** (**Scheme 4**) occurs with a positive change in free energy (21 kJ mol^{-1}; **Scheme 4**), indicating that $•O_2^-$ addition to 5-hydroxy-4-oxo-pentenal.H_2O to form 5-hydroxy-4-oxo-pentenal.H_2O/$•O_2^-$ is disfavored thermodynamically. The subsequent reactions that oxidize 5-hydroxy-4-oxo-pentenal.H_2O/$•O_2^-$ (**step 2-5; Scheme 4**), in contrast, occur with negative free energy changes (from -668 to -149 kJ mol^{-1}; **Scheme 4**), reflecting a thermodynamic driving force for 5-hydroxy-4-oxo-pentenal.H_2O/$•O_2^-$ oxidation once formed in **step 1** (**Scheme 4**).

The reactive nature of free radicals[54] suggests that the reactions that mediate 1,5,5-trihydroxy-2-oxo-pentan-4-yl-peroxyl• oxidation (**steps 3-5**; **Scheme 4**) occur at pseudo-steady state, as was concluded for the steps that mediate *ortho*-BA/•OH fragmentation (**Section 2.2**). The pseudo-steady-state nature of these reactions is supported by comparisons drawn between the calculated rate constants of elementary steps that comprise these groupings in **Scheme 4** (**Scheme S3**) with the rate constants for $•O_2^-$ addition to 5-hydroxy-4-oxo-pentenal.H_2O and 5-hydroxy-4-oxo-pentenal.H_2O/$•O_2^-$ protonation,

as discussed in **Section S11**. The pseudo-steady-state nature of these steps suggests that 1,5,5-trihydroxy-2-oxo-pentan-4-yl-peroxyl• is oxidized to oxalic acid (**steps 3-5**; **Scheme 4**) instantly once formed from 5-hydroxy-4-oxo-pentenal.H_2O/•O_2^- (**steps 2**; **Scheme 4**). The rate of 5-hydroxy-4-oxo-pentenal.H_2O/•O_2^- protonation (**step 2**; **Scheme 4**) therefore limits 5-hydroxy-4-oxo-pentenal.H_2O oxidation to oxalic acid through the steps in **Scheme 4**.

Oxalic acid forms at yields which increase linearly with time at the initial stages of the sonochemical benzyl alcohol oxidation process (< 1.1×10^4 s; **Fig. 1**). This constant rate of oxalic acid production indicates that the intermediates in oxalic acid formation are formed and consumed in rapid succession without accumulating to concentrations comparable to other oxidation products. Oxalic acid would otherwise form at an increasing rate as the concentrations of these reactive intermediates increase. Consequently, 5-hydroxy-4-oxo-pentenal.H_2O must be reactive enough even at low concentrations generated within the initial stages of benzyl alcohol oxidation to plausibly mediate oxalic acid formation through the steps in **Scheme 4**.

A kinetic model for 5-hydroxy-4-oxo-pentenal.H_2O formation from benzyl alcohol (**Fig. 3b**) and conversion to oxalic acid (**Scheme 4**) was constructed to simulate 5-hydroxy-4-oxo-pentenal.H_2O and oxalic acid concentrations during the initial stages of sonochemical benzyl alcohol oxidation. The irreversible nature of 5-hydroxy-4-oxo-pentenal.H_2O/•O_2^- protonation (as expected from the weak acidity of α-carbons in ketones; **step 2**; **Scheme 4**) taken together with the pseudo-steady-state oxidation of its protonated counterpart (1,5,5-trihydroxy-2-oxo-pentan-4-yl-peroxyl•; **steps 3-5**; **Scheme 4**) to oxalic acid (**Section S11**) suggests that the rate of oxalic acid formation equals the forward rate of 5-hydroxy-4-oxo-pentenal.H_2O/•O_2^- protonation ($r_{HOP\rightarrow OA}$). The rate of this protonation reaction ($r_{HOP\rightarrow OA}$) is proportional to the concentration of 5-hydroxy-4-oxo-pentenal.H_2O/•O_2^- ($[HOP/\bullet O_2^-]$) and of H^+ ($[H^+]$). Proton-transfer occurs between enolates and H^+ at rates that are near the limits of diffusion[66], indicating that the rate constant for this 5-hydroxy-4-oxo-pentenal.H_2O/•O_2^- protonation reaction reflects diffusion control (k_D; **Eq. S7**):

$$r_{HOP\rightarrow OA} = k_D[H^+][HOP/\bullet O_2^-] \quad (2)$$

A comparison between the DFT-derived rate constant for $\bullet O_2^-$ elimination from 5-hydroxy-4-oxo-pentenal.H_2O/$\bullet O_2^-$ (the reverse of **step 1**; **Scheme 4**) and the pseudo-first-order rate constant 5-hydroxy-4-oxo-pentenal.H_2O/$\bullet O_2^-$ protonation (**step 2**; **Scheme 4**), drawn in **Section S10**, shows that 5-hydroxy-4-oxo-pentenal.H_2O/$\bullet O_2^-$ forms in quasi-equilibrium with 5-hydroxy-4-oxo-pentenal.H_2O and $\bullet O_2^-$. This quasi-equilibrium concentration of 5-hydroxy-4-oxo-pentenal.H_2O/$\bullet O_2^-$ is related the concentrations of 5-hydroxy-4-oxo-pentenal.H_2O ($[HOP]$) and $\bullet O_2^-$ ($[\bullet O_2^-]$) by an equilibrium constant for the addition reaction (K_{HOP,O_2^-}; **step 1**; **Scheme 4**):

$$K_{HOP,O_2^-} = \frac{[HOP/\bullet O_2^-]}{[\bullet O_2^-][HOP]} \quad (3)$$

The rate of oxalic acid formation ($r_{HOP\rightarrow OA}$) can be related to the concentrations of 5-hydroxy-4-oxo-pentenal.H_2O and $\bullet O_2^-$ by replacing the $[HOP/\bullet O_2^-]$ term in **Equation 2** with its value from **Equation 3**:

$$r_{HOP\rightarrow OA} = K_{HOP,O_2^-} k_D [H^+][\bullet O_2^-][HOP] \quad (4)$$

The form of **Equation 4** shows that oxalic acid forms at a rate that is proportional to $\bullet O_2^-$, H^+, and 5-hydroxy-4-oxo-pentenal.H_2O concentrations.

Mixtures of $\bullet O_2^-$ and •OOH ($\bullet OOH/\bullet O_2^-$) form as a stoichiometric product of •OH-benzyl alcohol reactions (**Scheme 2** and **Fig. 3**). The stoichiometric formation of these species, combined with the conclusion that •OH-benzyl alcohol reactions are predominantly responsible for benzyl alcohol consumption during ultrasound irradiation (**Section 2.1**), suggests that the initial forward rate of $\bullet OOH/\bullet O_2^-$ formation ($r_{\bullet OOH/\bullet O_2^-}$) corresponds to the initial rate measured for benzyl alcohol consumption (1.9×10^{-8} M^{-1} s^{-1}; **Table S16**). $\bullet OOH/\bullet O_2^-$ terminate through either single-electron transfer between $\bullet O_2$ and •OOH (**Eq. 3**) or H-transfer between two •OOH (**Eq. 4**):

$$\bullet O_2^- + \bullet OOH \rightarrow O_2 + HOO^- \quad (5)$$

$$\bullet OOH + \bullet OOH \rightarrow O_2 + H_2O_2 \quad (6)$$

The second-order rate constants for these termination reactions (9.7×10^{7} M^{-1} s^{-1} for **Eq. 5** and 8.3×10^{5} M^{-1} s^{-1} for **Eq. 6**, at 298 K [35,67]) are large compared to $r_{\bullet OOH/\bullet O_2^-}$ (1.9×10^{-8} M^{-1} s^{-1}). The large rate constants for these termination reactions suggest that $\bullet OOH/\bullet O_2^-$ concentrations rapidly adjust to low pseudo-steady-state values that balance their formation from •OH-benzyl alcohol reactions, as shown

by a kinetic analysis in **Section S8**. An expression for these pseudo-steady state $\bullet O_2^-$ concentrations is obtained by equating the rate of $\bullet OOH/\bullet O_2^-$ formation (from •OH-benzyl alcohol reactions) and termination by **Equations 5** and **6**, as derived in **Section S8**:

$$[\bullet\, O_2^-] = \left(\frac{r_{\bullet OOH/\bullet O_2^-}}{\frac{k_{\bullet OOH,\bullet O_2^-}[H^+]}{K_{a,OOH}} + \frac{k_{2\bullet OOH}[H^+]^2}{K_{a,OOH}^2}} \right)^{\frac{1}{2}} \quad (7)$$

Here, $K_{a,OOH}$ is the acid dissociation constant for •OOH (4.9×10^{-3} at 315 K [34]), $k_{\bullet OOH,\bullet O_2^-}$ is the rate constant for $\bullet OOH$-$\bullet O_2^-$ electron transfer (**Eq. 5**), and $k_{2\bullet OOH}$ is the rate constant for •OOH-•OOH H-transfer (**Eq. 6**). **Equation 7** shows that $[\bullet\, O_2^-]$ concentrations depend inversely on H^+ concentrations, reflecting pH effect on equilibrium between $\bullet O_2^-$ and •OOH.

Time-dependent concentrations of 5-hydroxy-4-oxo-pentenal.H_2O ($[HOP]$), which influence oxalic acid formation rates through **Equation 4**, were described by equating the rate of 5-hydroxy-4-oxo-pentenal.H_2O accumulation ($d[HOP]/dt$) to the difference between its rate of formation by benzyl alcohol fragmentation ($r_{BA\rightarrow HOP}$) and consumption by oxidation to oxalic acid ($r_{HOP\rightarrow OA}$; **Eq. 2**):

$$\frac{d[HOP]}{dt} = r_{BA\rightarrow HOP} - r_{HOP\rightarrow OA} \quad (8)$$

This set of coupled equations (**Eqs. 4**, **7**, and **8**) were solved numerically to calculate time-dependent concentrations of 5-hydroxy-4-oxo-pentenal.H_2O and oxalic acid. $[H^+]$ was calculated by solving the system of algebraic equations for the deprotonation of acid products (oxalic and formic acid) at equilibrium (**Section S6**). Formic acid yields were assumed to be twice the yield of oxalic acid to reflect the stoichiometry of the proposed 5-hydroxy-4-oxo-pentenal.H_2O fragmentation mechanism (**Scheme 4**). The $r_{BA\rightarrow HOP}$ value was determined by regressing the predicted oxalic acid yields to measured values in the initial stages of the oxidation process (within 1.1×10^4 s) when both benzyl alcohol and oxalic acid concentrations changed linearly with time (**Fig. 1**). This regression was necessary because the amount of benzyl alcohol that fragmented specifically to 5-hydroxy-4-oxo-pentenal.H_2O (**steps 2c-2d**; **Scheme S1**) could not be assessed directly from the distributions of products measured during sonochemical experiments. An upper bound for the $r_{BA\rightarrow HOP}$ value was specified by the rate of benzyl alcohol consumption that was unaccounted for by yields of products with the aromatic ring intact

(9.0×10^{-9} M s^{-1}; **Table S16**). The regressed $r_{BA\rightarrow HOP}$ values are shown in **Table S17**. The concentrations of 5-hydroxy-4-oxo-pentenal.H_2O and oxalic acid are shown in **Figures 4a** and **4b**, respectively, calculated using different values of $K_{HOP,\bullet O_2^-}$ (4.0×10^{-4} to 4.0 M^{-1}). The lower bound of $K_{HOP,\bullet O_2^-}$ reflects the value calculated using DFT (**Table S10**). **Figure 4b** also shows the measured yields of oxalic acid reported in **Figure 1** for comparison.

The 5-hydroxy-4-oxo-pentenal.H_2O concentrations calculated with the smaller $K_{HOP,\bullet O_2^-}$ values (4.0×10^{-4} to 4.0×10^{-3} M^{-1}) increased monotonically with reaction time, ultimately exceeding 10^{-4} M at longer reaction times. At larger $K_{HOP,\bullet O_2^-}$ values (4.0×10^{-2} to 4.0 M^{-1}), 5-hydroxy-4-oxo-pentenal.H_2O concentrations peaked below 5×10^{-5} M with increasing reaction time. This peak occurred at earlier reaction times and at lower concentrations as $K_{HOP,\bullet O_2^-}$ increased. The peak 5-hydroxy-4-oxo-pentenal.H_2O concentration emerges when $K_{HOP,\bullet O_2^-}$ values increase because of a concomitant increase in $r_{HOP\rightarrow OA}$ (**Eq. 4**), which ultimately exceeds $r_{BA\rightarrow HOP}$ values (**Table S16**) as 5-hydroxy-4-oxo-pentenal.H_2O accumulates.

The calculated oxalic acid concentrations increased monotonically with reaction time for all $K_{HOP,\bullet O_2^-}$ values considered (**Fig. 4b**). The oxalic acid concentrations calculated using the DFT value for $K_{HOP,\bullet O_2^-}$ (4.0×10^{-4} M^{-1}) were negligible compared to the measured yields (**Fig. 4b**). Oxalic acid concentrations calculated with the larger $K_{HOP,\bullet O_2^-}$ values of 2.0 M^{-1} and 4.0 M^{-1}, however, were in close agreement (within 27% and 17%, respectively) with measured yields. The $r_{BA\rightarrow HOP}$ values needed for these predictions ($6.7(\pm2.0)\times10^{-9}$ M s^{-1} and $6.4(\pm1.2)\times10^{-9}$ M s^{-1}, respectively) were less than the rate of benzyl alcohol consumption to the non-aromatic products (9.0×10^{-9} M s^{-1}; **Table S16**), and are therefore consistent with the amounts of benzyl alcohol converted by ultrasound irradiation.

The ratios between the $K_{HOP,\bullet O_2^-}$ values needed to accurately predict oxalic acid yields (2.0 M^{-1} and 4.0 M^{-1}; **Fig. 4**) and the DFT-derived $K_{HOP,\bullet O_2^-}$ value (4.0×10^{-4} M^{-1}) correspond to differences in free energy for the $\bullet O_2^-$ and 5-hydroxy-4-oxo-pentenal.H_2O reaction (**step 1**; **Scheme 4**) of -16 kJ mol^{-1} ($K_{HOP,\bullet O_2^-}$ =2.0 M^{-1}) and -18 kJ mol^{-1} ($K_{HOP,\bullet O_2^-}$ =4.0 M^{-1}). This difference in free energy is reasonable considering the absolute errors associated with predicting the free energies of ions in solution using the

SMD solvation model[48] (17 kJ mol^{-1}), and the errors for predicting entropy changes for bimolecular reactions in solution using implicit solvation models[68].

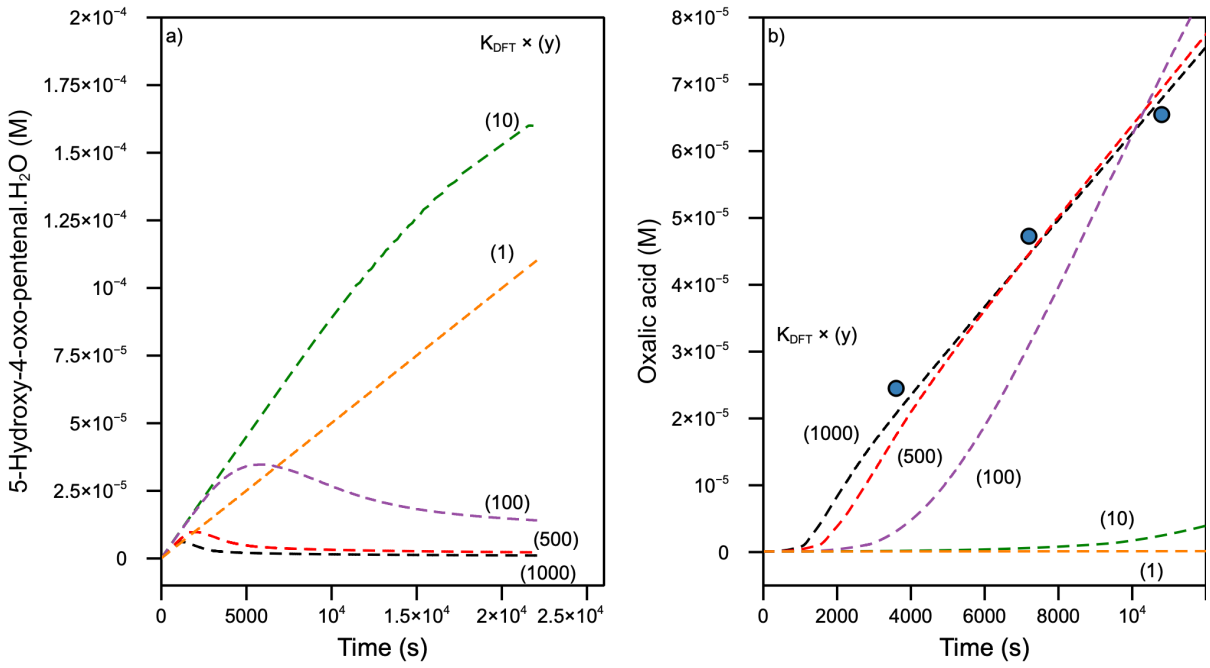

Figure 4: The concentrations of 5-hydroxy-4-oxo-pentenal.H_2O (a; dashed curves) and oxalic acid (b; dashed curves) during •OH-benzyl alcohol reactions (at 315 K) calculated using **Equations 4**, **7**, and **8.** Different values for the equilibrium constants for the $•O_2^-$-5-hydroxy-4-oxo-pentenal.H_2O reaction ($K_{HOP,•O_2^-}$; **step 1**; **Scheme 3**) relative to its DFT-derived value (4.0×10^{-4} M^{-1}; K_{DFT}; **Table S10**) were used and shown in different colors. The measured oxalic acid concentrations from **Figure 1** (circles). The pH was calculated from equilibrated deprotonation of oxalic acid and formic acid products (**Section S7**). The $r_{BA\rightarrow HOP}$ values in **Equation 4** were regressed to the measured oxalic acid concentrations, and reported in **Table S17**.

Figure 4b represents an agreement between measured oxalic acid yields and predictions from the kinetic model. This agreement demonstrates that the proposed fragmentation of benzyl alcohol to 5-hydroxy-4-oxo-pentenal.H_2O through mechanisms established in gas-phase chemistry (**Fig. 3b**) and its subsequent oxidation mediated by $•O_2^-$ (**Scheme 4**) together explain how oxalic acid forms during sonochemical benzyl alcohol oxidation. The pathway involving $•O_2^-$ addition to the electrophilic

aldehyde, ketone, and unsaturated ketone functions requires a protic solvent (H_2O) for •OOH deprotonation to $•O_2^-$. The nucleophilic reactions of $•O_2^-$ consequently drive significant oxalic acid production from aqueous •OH-initiated benzyl alcohol oxidation processes in sonochemical reactors, unlike in the gas-phase where oxalic acid is not observed[28,30,45].

5-hydroxy-4-oxo-pentenal.H_2O is oxidized by $•O_2^-$ (**Scheme 4**) without involving •OH, thereby preserving the •OH for initiating benzyl alcohol oxidation. These $•O_2^-$ reactions therefore reduce the number of •OH initiators needed to oxidize benzyl alcohol and its oxidation products, thus lowering the operational costs associated with generating •OH. Furthermore, •OOH (and $•O_2^-$ by inference) has been reported as an intermediate in •OH-initiated oxidation reactions of aqueous aldehydes[39–41] (hydrates), alcohols[41,42], α-β ketals[39,40], organic acids[41,43], and arenes[24,26]. This ability for •OOH and $•O_2^-$ to form in such diverse •OH-initiated aqueous oxidation reactions suggests that nucleophilic $•O_2^-$ reactions with unsaturated ketones, ketones, and aldehydes, shown here in the context of benzyl alcohol oxidation, may propagate analogous reactions in advanced oxidation processes of water contaminated by diverse organic pollutants. Designing oxidation processes that harness these $•O_2^-$ propagation reactions can therefore help make •OH-based oxidation processes cost-effective and scalable for treating municipal, industrial, and agricultural wastewaters.

3. Conclusions

Low frequency ultrasound irradiation (20 kHz) is shown to oxidize aqueous benzyl alcohol in an O_2-rich environment through pathways initiated by •OH, forming benzaldehyde, phenol, hydroxymethyl-phenol isomers, and oxalic acid as the predominant products. Mechanistic inquiries into •OH-benzyl alcohol reactions and kinetic assessments of elementary steps using density functional theory indicate that these products result from rapid sequences of radical reactions occurring at pseudo-steady state. Aromatic benzyl alcohol substitution is mediated by •OH addition to the aromatic ring at *ipso*, *ortho*, *meta*, and *para* positions relative to the hydroxymethyl- function, forming benzyl alcohol-•OH adducts. The *ipso* adduct eliminates hydroxymethyl• yielding phenol, while *ortho*, *meta*, and *para* adducts transfer H• to O_2, forming hydroxymethyl-phenol isomers and •OOH. Through parallel pathways, these benzyl alcohol-•OH adducts mediate the de-aromatization and fragmentation of benzyl

alcohol to α-carbonyl-aldehyde (i.e., glyoxal or 3-hydroxy-2-oxopropanal) and γ-carbonyl-alk-2-enal (i.e., but-2-enedial, 2-hydroxymethyl-but-2-enedial, or 5-hydroxy-4-oxo-pent-2-enal) products. These fragmentation pathways follow similar mechanisms to those established for aromatic compounds in the gas phase.

$\bullet O_2^-$, which forms as a byproduct of •OH-benzyl alcohol reactions, is found to activate the hydrated form of 5-hydroxy-4-oxo-pentenal by adding to its α-β unsaturated carbonyl function. The nucleophilic addition initiates radical-chain propagation reactions that sequentially cleave 3 C-C bonds yielding oxalic acid, formic acid, and formaldehyde, and regenerate $\bullet O_2^-$. This sequence is mediated by nucleophilic additions of $\bullet O_2^-$ to ketone and aldehyde functions of 5-hydroxy-4-oxo-pentenal-derived intermediates. Kinetic analyses of these 5-hydroxy-4-oxo-pentenal oxidation reactions show that they provide a feasible route to oxalic acid during sonochemical benzyl alcohol oxidation. These $\bullet O_2^-$ reactions require a protic solvent to stabilize the charged $\bullet O_2^-$ species, and therefore accounts for oxalic acid formation from benzyl alcohol oxidation in the aqueous phase, unlike in the gas-phase.

The nucleophilic reactions of $\bullet O_2^-$ uncovered in mechanisms for benzyl alcohol oxidation reveals $\bullet O_2^-$ to be a potent initiator for degrading unsaturated carbonyls, ketones, and aldehydes in aqueous solutions. These $\bullet O_2^-$ reactions do not consume •OH, thereby degrading carbonyl-containing molecules while preserving •OH for reaction with refractory molecules. Leveraging such $\bullet O_2^-$ reactions offers a promising strategy to reduce the energy and chemical demands of advanced oxidation processes, thus promoting their sustainable and scalable application in wastewater treatment.

Associated content

Supporting Information

Experimental and computational methods (**Sections S1** and **S2**); scheme showing proposed fragmentation products (**Section S3**); the mechanism, kinetics, and thermodynamics of benzene fragmentation (**Section S4**); kinetic analyses of benzyl alcohol fragmentation (**Section S5**), superoxide formation (**Section S7**), and 5-hydroxy-4-oxo-pentenal oxidation (**Sections S8, S10**, and **S11**); the pH calculation from benzyl alcohol oxidation products (**Section S6**); a comprehensive mechanism for 5-hydroxy-4-oxo-pentenal oxidation (**Section S9**); tabulated thermodynamic and kinetic parameters for

oxidation reactions (**Section S12**); tabulated imaginary frequencies and tunneling corrections (**Section S13**); thermochemistry for anion association reactions (**Section S14**); rate data from benzyl alcohol oxidation measurements (**Section S15**); regression analysis for the kinetic model for oxalic acid formation (**Section S16**); and additional references. These materials are contained within **Sections S1-S16**, **Figures S1-S2**, **Schemes S1-S3**, **Tables S1-S17**, and **Equations S1-S28**.

The authors have cited additional references within the Supporting Information.

Code and data availability

All density functional theory output files and original codes used for their analysis are openly available: https://github.com/ari-fischer/benzyl_alcohol_oxidation_2024. These output files and codes include: DFT output files for convergence to stationary points, vibrational frequency analysis, and intrinsic reaction coordinate analysis; Jupyter notebook and dependences needed to generate thermochemical datasets from DFT outputs; molecular volumes calculated from optimized geometries; MATLAB code for predicting experimental product yields; and SMILES representations of reaction networks.

Acknowledgements

This research is supported by the National Research Foundation, Prime Minister's Office, Singapore under its Campus for Research Excellence and Technological Enterprise (CREATE) programme. This work is also supported by the Ministry of Research Academic Research Fund Tier-1: RG87/23. Additional support comes from joint funding from the NRF and the French National Research Agency (ANR) through the NRF-ANR Joint Research Project (NRF2020-NRF-ANR066 SonoNanoCat ANR-20-CE09-0030). Support is also provided for Dr. Teseer Bahry, Dr. François Jérôme, Dr. Sabine Valange and Dr. Prince N. Amaniampong from the European Union (ERDF) and Région Nouvelle Aquitaine. The Engineering and Physical Sciences Research Council of the UK (Grant number EP/W012316/1) also supports this project. The authors also acknowledge technical assistance and computing resources from the High-Performance Computing (HPC) Centre, NTU.

Author Information

Corresponding Author

tej.choksi@ntu.edu.sg and prince.nana.amaniampong@univ-poitiers.fr

Notes

The authors declare no competing financial interests.

Author Contributions

Conceptualization: AF and TC conceptualized the mechanistic descriptions and computational modeling approaches. *Data curation:* AF curated original code and data repository. *Formal analysis:* AF analyzed the DFT calculations and kinetic data; TB analyzed the experimental kinetic data; ZX analyzed EPR data. *Funding acquisition:* Financial support was acquired by PA, SV, TC, and WL. *Investigation:* AF conducted the computational study, TB conducted the kinetic measurements, and ZX conducted the EPR measurements. *Methodology:* AF and TC designed the computational studies. PA, TB, and RJ designed the kinetic experiments. KQ, RL, WL, and ZX designed the EPR experiments. *Project administration:* The research activities were coordinated by PA, SV, TC, and WL. *Resources:* Computational resources were provided by TC, resources for kinetic experiments by FJ, SV, and PA, and experimental resources for EPR measurements by RL and WL. *Supervision:* The computational research was supervised by TC, kinetic experiments by FJ, SV, and PA, and EPR studies by RL and WL. *Visualization:* The figures for EPR data were made by ZX. AF made all other figures. *Writing-original draft:* The original manuscript was drafted by AF and TC. *Writing-review & editing:* The manuscript was edited and reviewed by all authors.

References

(1) Fatone, F.; Di Fabio, S.; Bolzonella, D.; Cecchi, F. Fate of Aromatic Hydrocarbons in Italian Municipal Wastewater Systems: An Overview of Wastewater Treatment Using Conventional Activated-Sludge Processes (CASP) and Membrane Bioreactors (MBRs). *Water Research* **2011**, *45* (1), 93–104. https://doi.org/10.1016/j.watres.2010.08.011.

(2) Hofmann, K.; Hammer, E. Anaerobic Formation and Degradation of Toxic Aromatic Compounds in Agricultural and Communal Sewage Deposits. *Chemosphere* **1999**, *38* (11), 2561–2568. https://doi.org/10.1016/S0045-6535(98)00463-9.

(3) Halling-Sørensen, B.; Nors Nielsen, S.; Lanzky, P. F.; Ingerslev, F.; Holten Lützhøft, H. C.; Jørgensen, S. E. Occurrence, Fate and Effects of Pharmaceutical Substances in the Environment- A Review. *Chemosphere* **1998**, *36* (2), 357–393. https://doi.org/10.1016/S0045-6535(97)00354-8.

(4) Kolpin, D. W.; Furlong, E. T.; Meyer, M. T.; Thurman, E. M.; Zaugg, S. D.; Barber, L. B.; Buxton, H. T. Pharmaceuticals, Hormones, and Other Organic Wastewater Contaminants in U.S. Streams, 1999−2000: A National Reconnaissance. *Environ. Sci. Technol.* **2002**, *36* (6), 1202–1211. https://doi.org/10.1021/es011055j.
(5) Stepnowski, P.; Siedlecka, E. M.; Behrend, P.; Jastorff, B. Enhanced Photo-Degradation of Contaminants in Petroleum Refinery Wastewater. *Water Research* **2002**, *36* (9), 2167–2172. https://doi.org/10.1016/S0043-1354(01)00450-X.
(6) Moore, J. W.; Ramamoorthy, S. Aromatic Hydrocarbons—Monocyclics. In *Organic Chemicals in Natural Waters*; Springer Series on Environmental Management; Springer New York: New York, NY, 1984; pp 43–66. https://doi.org/10.1007/978-1-4613-9538-6_4.
(7) Xia, J.; Sun, H.; Zhang, X.; Zhang, T.; Ren, H.; Ye, L. Aromatic Compounds Lead to Increased Abundance of Antibiotic Resistance Genes in Wastewater Treatment Bioreactors. *Water Research* **2019**, *166*, 115073. https://doi.org/10.1016/j.watres.2019.115073.
(8) Fent, K.; Weston, A.; Caminada, D. Ecotoxicology of Human Pharmaceuticals. *Aquatic Toxicology* **2006**, *76* (2), 122–159. https://doi.org/10.1016/j.aquatox.2005.09.009.
(9) Ameta, S. C. Introduction. In *Advanced Oxidation Processes for Waste Water Treatment*; Elsevier, 2018; pp 1–12. https://doi.org/10.1016/B978-0-12-810499-6.00001-2.
(10) Bein, E.; Seiwert, B.; Reemtsma, T.; Drewes, J. E.; Hübner, U. Advanced Oxidation Processes for Removal of Monocyclic Aromatic Hydrocarbon from Water: Effects of O_3/H_2O_2 and UV/H_2O_2 Treatment on Product Formation and Biological Post-Treatment. *Journal of Hazardous Materials* **2023**, *450*, 131066. https://doi.org/10.1016/j.jhazmat.2023.131066.
(11) Deng, Y.; Zhao, R. Advanced Oxidation Processes (AOPs) in Wastewater Treatment. *Curr Pollution Rep* **2015**, *1* (3), 167–176. https://doi.org/10.1007/s40726-015-0015-z.
(12) Ma, D.; Yi, H.; Lai, C.; Liu, X.; Huo, X.; An, Z.; Li, L.; Fu, Y.; Li, B.; Zhang, M.; Qin, L.; Liu, S.; Yang, L. Critical Review of Advanced Oxidation Processes in Organic Wastewater Treatment. *Chemosphere* **2021**, *275*, 130104. https://doi.org/10.1016/j.chemosphere.2021.130104.
(13) Pignatello, J. J.; Oliveros, E.; MacKay, A. Advanced Oxidation Processes for Organic Contaminant Destruction Based on the Fenton Reaction and Related Chemistry. *Critical Reviews in Environmental Science and Technology* **2006**, *36* (1), 1–84. https://doi.org/10.1080/10643380500326564.
(14) Torres-Palma, R. A.; Serna-Galvis, E. A. Sonolysis. In *Advanced Oxidation Processes for Waste Water Treatment*; Elsevier, 2018; pp 177–213. https://doi.org/10.1016/B978-0-12-810499-6.00007-3.
(15) Rayaroth, M. P.; Aravind, U. K.; Aravindakumar, C. T. Degradation of Pharmaceuticals by Ultrasound-Based Advanced Oxidation Process. *Environ Chem Lett* **2016**, *14* (3), 259–290. https://doi.org/10.1007/s10311-016-0568-0.
(16) Berlan, J.; Trabelsi, F.; Delmas, H.; Wilhelm, A. M.; Petrignani, J. F. Oxidative Degradation of Phenol in Aqueous Media Using Ultrasound. *Ultrasonics Sonochemistry* **1994**, *1* (2), S97–S102. https://doi.org/10.1016/1350-4177(94)90005-1.
(17) Sharma, A.; Bapat, P. S.; Gogate, P. R.; Gastgar, S. N.; Pandit, A. B. Process Intensification of Hydrogenation Reactions Using Cavitation: Modelling the Effect of Solvent and Catalyst. *Chemical Engineering and Processing: Process Intensification* **2009**, *48* (1), 432–437. https://doi.org/10.1016/j.cep.2008.05.008.
(18) Gogate, P. R.; Pandit, A. B. Sonochemical Reactors: Scale up Aspects. *Ultrasonics Sonochemistry* **2004**, *11* (3–4), 105–117. https://doi.org/10.1016/j.ultsonch.2004.01.005.
(19) Miklos, D. B.; Remy, C.; Jekel, M.; Linden, K. G.; Drewes, J. E.; Hübner, U. Evaluation of Advanced Oxidation Processes for Water and Wastewater Treatment – A Critical Review. *Water Research* **2018**, *139*, 118–131. https://doi.org/10.1016/j.watres.2018.03.042.
(20) Rosenfeldt, E. J.; Linden, K. G.; Canonica, S.; Von Gunten, U. Comparison of the Efficiency of OH Radical Formation during Ozonation and the Advanced Oxidation Processes O_3/H_2O_2 and UV/H_2O_2. *Water Research* **2006**, *40* (20), 3695–3704. https://doi.org/10.1016/j.watres.2006.09.008.
(21) Lee, Y.; Von Gunten, U. Advances in Predicting Organic Contaminant Abatement during Ozonation of Municipal Wastewater Effluent: Reaction Kinetics, Transformation Products, and

Changes of Biological Effects. *Environ. Sci.: Water Res. Technol.* **2016**, *2* (3), 421–442. https://doi.org/10.1039/C6EW00025H.
(22) Mousset, E.; Loh, W. H.; Lim, W. S.; Jarry, L.; Wang, Z.; Lefebvre, O. Cost Comparison of Advanced Oxidation Processes for Wastewater Treatment Using Accumulated Oxygen-Equivalent Criteria. *Water Research* **2021**, *200*, 117234. https://doi.org/10.1016/j.watres.2021.117234.
(23) Hübner, U.; Spahr, S.; Lutze, H.; Wieland, A.; Rüting, S.; Gernjak, W.; Wenk, J. Advanced Oxidation Processes for Water and Wastewater Treatment – Guidance for Systematic Future Research. *Heliyon* **2024**, *10* (9), e30402. https://doi.org/10.1016/j.heliyon.2024.e30402.
(24) Pan, X.-M.; Schuchmann, M. N.; Von Sonntag, C. Oxidation of Benzene by the OH Radical. A Product and Pulse Radiolysis Study in Oxygenated Aqueous Solution. *J. Chem. Soc., Perkin Trans. 2* **1993**, No. 3, 289. https://doi.org/10.1039/p29930000289.
(25) Al-Sheikhly, M.; Poster, D. L.; An, J.-C.; Neta, P.; Silverman, J.; Huie, R. E. Ionizing Radiation-Induced Destruction of Benzene and Dienes in Aqueous Media. *Environ. Sci. Technol.* **2006**, *40* (9), 3082–3088. https://doi.org/10.1021/es052533j.
(26) Dong, P.; Chen, Z.; Qin, X.; Gong, Y. Water Significantly Changes the Ring-Cleavage Process During Aqueous Photooxidation of Toluene. *Environ. Sci. Technol.* **2021**, *55* (24), 16316–16325. https://doi.org/10.1021/acs.est.1c04770.
(27) Wang, L.; Wu, R.; Xu, C. Atmospheric Oxidation Mechanism of Benzene. Fates of Alkoxy Radical Intermediates and Revised Mechanism. *J. Phys. Chem. A* **2013**, *117* (51), 14163–14168. https://doi.org/10.1021/jp4101762.
(28) Wang, L. The Atmospheric Oxidation Mechanism of Benzyl Alcohol Initiated by OH Radicals: The Addition Channels. *ChemPhysChem* **2015**, *16* (7), 1542–1550. https://doi.org/10.1002/cphc.201500012.
(29) Harrison, J. C.; Wells, J. R. Gas-Phase Chemistry of Benzyl Alcohol: Reaction Rate Constants and Products with OH Radical and Ozone. *Atmospheric Environment* **2009**, *43* (4), 798–804. https://doi.org/10.1016/j.atmosenv.2008.11.001.
(30) Bernard, F.; Magneron, I.; Eyglunent, G.; Daële, V.; Wallington, T. J.; Hurley, M. D.; Mellouki, A. Atmospheric Chemistry of Benzyl Alcohol: Kinetics and Mechanism of Reaction with OH Radicals. *Environ. Sci. Technol.* **2013**, *47* (7), 3182–3189. https://doi.org/10.1021/es304600z.
(31) Atkinson, R.; Arey, J. Atmospheric Degradation of Volatile Organic Compounds. *Chem. Rev.* **2003**, *103* (12), 4605–4638. https://doi.org/10.1021/cr0206420.
(32) Olivella, S.; Solé, A.; Bofill, J. M. Theoretical Mechanistic Study of the Oxidative Degradation of Benzene in the Troposphere: Reaction of Benzene−HO Radical Adduct with O_2. *J. Chem. Theory Comput.* **2009**, *5* (6), 1607–1623. https://doi.org/10.1021/ct900082g.
(33) Klotz, B.; Volkamer, R.; Hurley, M. D.; Andersen, M. P. S.; Nielsen, O. J.; Barnes, I.; Imamura, T.; Wirtz, K.; Becker, K.-H.; Platt, U.; Wallington, T. J.; Washida, N. OH-Initiated Oxidation of Benzene. *Phys. Chem. Chem. Phys.* **2002**, *4* (18), 4399–4411. https://doi.org/10.1039/b204398j.
(34) Behar, D.; Czapski, G.; Rabani, J.; Dorfman, L. M.; Schwarz, H. A. Acid Dissociation Constant and Decay Kinetics of the Perhydroxyl Radical. *J. Phys. Chem.* **1970**, *74* (17), 3209–3213. https://doi.org/10.1021/j100711a009.
(35) Bielski, B. H. J.; Cabelli, D. E.; Arudi, R. L.; Ross, A. B. Reactivity of HO_2/O^-_2 Radicals in Aqueous Solution. *Journal of Physical and Chemical Reference Data* **1985**, *14* (4), 1041–1100. https://doi.org/10.1063/1.555739.
(36) Danen, W. C.; Warner, J. The Remarkable Nucleophilicity of Superoxide Anion Radical. Rate Constants for Reaction of Superoxide Ion with Aliphatic Bromides. *Tetrahedron Letters* **1977**, *11*, 989–992.
(37) Dietz, R.; Forno, A. E. J.; Larcombe, B. E.; Peover, M. E. Nucleophilic Reactions of Electrogenerated Superoxide Ion. *J. Chem. Soc., B:* **1970**, 816. https://doi.org/10.1039/j29700000816.
(38) Fischer, A.; Bahry, T.; Xie, Z.; Qian, K.; Li, R.; Kwan, J.; Jerome, F.; Valange, S.; Liu, W.; Amaniampong, P.; Choksi, T. S. Harnessing Ultrasound-derived Hydroxyl Radicals for the Selective Oxidation of Aldehyde Functions. *ChemSusChem* **2024**, e202400838. https://doi.org/10.1002/cssc.202400838.

(39) Lim, Y. B.; Tan, Y.; Turpin, B. J. Chemical Insights, Explicit Chemistry, and Yields of Secondary Organic Aerosol from OH Radical Oxidation of Methylglyoxal and Glyoxal in the Aqueous Phase. *Atmos. Chem. Phys.* **2013**, *13* (17), 8651–8667. https://doi.org/10.5194/acp-13-8651-2013.
(40) Tan, Y.; Carlton, A. G.; Seitzinger, S. P.; Turpin, B. J. SOA from Methylglyoxal in Clouds and Wet Aerosols: Measurement and Prediction of Key Products. *Atmospheric Environment* **2010**, *44* (39), 5218–5226. https://doi.org/10.1016/j.atmosenv.2010.08.045.
(41) Pandis, S. N.; Seinfeld, J. H. Sensitivity Analysis of a Chemical Mechanism for Aqueous-phase Atmospheric Chemistry. *J. Geophys. Res.* **1989**, *94* (D1), 1105–1126. https://doi.org/10.1029/JD094iD01p01105.
(42) Monod, A.; Chebbi, A.; Durand-Jolibois, R.; Carlier, P. Oxidation of Methanol by Hydroxyl Radicals in Aqueous Solution under Simulated Cloud Droplet Conditions. *Atmospheric Environment* **2000**, *34* (29–30), 5283–5294. https://doi.org/10.1016/S1352-2310(00)00191-6.
(43) Scholes, G.; Willson, R., L. Y-Radiolysis of Aqueous Thymine Solutions. Determination of Relative Reaction Rates of OH Radicals. *Transactions of the Faraday Society* **1967**, *63*, 2983–2993.
(44) Mark, G.; Tauber, A.; Laupert, R.; Schuchmann, H.-P.; Schulz, D.; Mues, A.; Von Sonntag, C. OH-Radical Formation by Ultrasound in Aqueous Solution – Part II: Terephthalate and Fricke Dosimetry and the Influence of Various Conditions on the Sonolytic Yield. *Ultrasonics Sonochemistry* **1998**, *5* (2), 41–52. https://doi.org/10.1016/S1350-4177(98)00012-1.
(45) Harrison, J. C.; Wells, J. R. Gas-Phase Chemistry of Benzyl Alcohol: Reaction Rate Constants and Products with OH Radical and Ozone. *Atmospheric Environment* **2009**, *43* (4), 798–804. https://doi.org/10.1016/j.atmosenv.2008.11.001.
(46) Shao, Y.; Gan, Z.; Epifanovsky, E.; Gilbert, A. T. B.; Wormit, M.; Kussmann, J.; Lange, A. W.; Behn, A.; Deng, J.; Feng, X.; Ghosh, D.; Goldey, M.; Horn, P. R.; Jacobson, L. D.; Kaliman, I.; Khaliullin, R. Z.; Kuś, T.; Landau, A.; Liu, J.; Proynov, E. I.; Rhee, Y. M.; Richard, R. M.; Rohrdanz, M. A.; Steele, R. P.; Sundstrom, E. J.; Woodcock, H. L.; Zimmerman, P. M.; Zuev, D.; Albrecht, B.; Alguire, E.; Austin, B.; Beran, G. J. O.; Bernard, Y. A.; Berquist, E.; Brandhorst, K.; Bravaya, K. B.; Brown, S. T.; Casanova, D.; Chang, C.-M.; Chen, Y.; Chien, S. H.; Closser, K. D.; Crittenden, D. L.; Diedenhofen, M.; DiStasio, R. A.; Do, H.; Dutoi, A. D.; Edgar, R. G.; Fatehi, S.; Fusti-Molnar, L.; Ghysels, A.; Golubeva-Zadorozhnaya, A.; Gomes, J.; Hanson-Heine, M. W. D.; Harbach, P. H. P.; Hauser, A. W.; Hohenstein, E. G.; Holden, Z. C.; Jagau, T.-C.; Ji, H.; Kaduk, B.; Khistyaev, K.; Kim, J.; Kim, J.; King, R. A.; Klunzinger, P.; Kosenkov, D.; Kowalczyk, T.; Krauter, C. M.; Lao, K. U.; Laurent, A. D.; Lawler, K. V.; Levchenko, S. V.; Lin, C. Y.; Liu, F.; Livshits, E.; Lochan, R. C.; Luenser, A.; Manohar, P.; Manzer, S. F.; Mao, S.-P.; Mardirossian, N.; Marenich, A. V.; Maurer, S. A.; Mayhall, N. J.; Neuscamman, E.; Oana, C. M.; Olivares-Amaya, R.; O'Neill, D. P.; Parkhill, J. A.; Perrine, T. M.; Peverati, R.; Prociuk, A.; Rehn, D. R.; Rosta, E.; Russ, N. J.; Sharada, S. M.; Sharma, S.; Small, D. W.; Sodt, A.; Stein, T.; Stück, D.; Su, Y.-C.; Thom, A. J. W.; Tsuchimochi, T.; Vanovschi, V.; Vogt, L.; Vydrov, O.; Wang, T.; Watson, M. A.; Wenzel, J.; White, A.; Williams, C. F.; Yang, J.; Yeganeh, S.; Yost, S. R.; You, Z.-Q.; Zhang, I. Y.; Zhang, X.; Zhao, Y.; Brooks, B. R.; Chan, G. K. L.; Chipman, D. M.; Cramer, C. J.; Goddard, W. A.; Gordon, M. S.; Hehre, W. J.; Klamt, A.; Schaefer, H. F.; Schmidt, M. W.; Sherrill, C. D.; Truhlar, D. G.; Warshel, A.; Xu, X.; Aspuru-Guzik, A.; Baer, R.; Bell, A. T.; Besley, N. A.; Chai, J.-D.; Dreuw, A.; Dunietz, B. D.; Furlani, T. R.; Gwaltney, S. R.; Hsu, C.-P.; Jung, Y.; Kong, J.; Lambrecht, D. S.; Liang, W.; Ochsenfeld, C.; Rassolov, V. A.; Slipchenko, L. V.; Subotnik, J. E.; Van Voorhis, T.; Herbert, J. M.; Krylov, A. I.; Gill, P. M. W.; Head-Gordon, M. Advances in Molecular Quantum Chemistry Contained in the Q-Chem 4 Program Package. *Molecular Physics* **2015**, *113* (2), 184–215. https://doi.org/10.1080/00268976.2014.952696.
(47) Mardirossian, N.; Head-Gordon, M. ωB97M-V: A Combinatorially Optimized, Range-Separated Hybrid, Meta-GGA Density Functional with VV10 Nonlocal Correlation. *The Journal of Chemical Physics* **2016**, *144* (21), 214110. https://doi.org/10.1063/1.4952647.
(48) Marenich, A. V.; Cramer, C. J.; Truhlar, D. G. Universal Solvation Model Based on Solute Electron Density and on a Continuum Model of the Solvent Defined by the Bulk Dielectric

Constant and Atomic Surface Tensions. *J. Phys. Chem. B* **2009**, *113* (18), 6378–6396. https://doi.org/10.1021/jp810292n.
(49) Eyring, H. The Activated Complex in Chemical Reactions. *The Journal of chemical physics* **1935**, *3* (2), 107–115. https://doi.org/10.1063/1.1749604.
(50) Peters, B. Transition State Theory. In *Reaction Rate Theory and Rare Events Simulations*; Elsevier, 2017; pp 227–271.
(51) Peters, B. Diffusion Control. In *Reaction Rate Theory and Rare Events Simulations*; Elsevier, 2017; pp 129–145.
(52) Smoluchowski, M. v. Versuch Einer Mathematischen Theorie Der Koagulationskinetik Kolloider Lösungen. *Zeitschrift für Physikalische Chemie* **1918**, *92U* (1), 129–168. https://doi.org/doi:10.1515/zpch-1918-9209.
(53) Buxton, G. V.; Greenstock, C. L.; Helman, W. P.; Ross, A. B. Critical Review of Rate Constants for Reactions of Hydrated Electrons, Hydrogen Atoms and Hydroxyl Radicals (·OH/·O⁻) in Aqueous Solution. *Journal of Physical and Chemical Reference Data* **1988**, *17* (2), 513–886. https://doi.org/10.1063/1.555805.
(54) Mill, T.; Hendry, D. G. Kinetics and Mechanisms of Free Radical Oxidation of Alkanes and Olefins in the Liquid Phase. *Comprehensive Chemical Kinetics* **1980**, *16*, 1–87. https://doi.org/10.1016/S0069-8040(08)70036-0.
(55) Peters, B. Rate Laws. In *Reaction Rate Theory and Rare Events Simulations*; Elsevier, 2017; pp 39–77. https://doi.org/10.1016/B978-0-44-456349-1.00003-9.
(56) Bowen, J. R.; Acrios, A.; Oppenheim, A. K. Singular Perturbation Refinement to Quasi-Steady State Approximation in Chemical Kinetics. *Chemical Engineering Sciences* **1963**, *18*, 177–188. https://doi.org/10.1016/0009-2509(63)85003-4.
(57) Atkinson, R. Atmospheric Chemistry of VOCs and NO_x. *Atmospheric Environment* **2000**. https://doi.org/10.1016/S1352-2310(99)00460-4.
(58) Galano, A.; Alvarez-Idaboy, J. R.; Ruiz-Santoyo, Ma. E.; Vivier-Bunge, A. Mechanism and Kinetics of the Reaction of OH Radicals with Glyoxal and Methylglyoxal: A Quantum Chemistry+CVT/SCT Approach. *ChemPhysChem* **2004**, *5* (9), 1379–1388. https://doi.org/10.1002/cphc.200400127.
(59) Wu, R.; Pan, S.; Li, Y.; Wang, L. Atmospheric Oxidation Mechanism of Toluene. *J. Phys. Chem. A* **2014**, *118* (25), 4533–4547. https://doi.org/10.1021/jp500077f.
(60) Manion, J. A.; Huie, R. E.; Levin, R. D.; Burgess Jr, D. R.; Orkin, W. L.; Tsang, W.; McGivern, W. S.; Hudgens, J. W.; Knyazev, V. D.; Atkinson, D. B.; Chai, E.; Tereza, A. M.; Lin, C.-Y.; Allison, T. C.; Mallard, W. G.; Westley, F.; Herron, J. T.; Hampson, R. F.; Frizzell, D. H. *NIST Chemical Kinetics Database, NIST Standard Reference Database 17, Version 7.0 (Web Version), Release 1.6.8, Data version 2015.09, National Institute of Standards and Technology, Gaithersburg, Maryland, 20899-8320.* https://kinetics.nist.gov/.
(61) Neta, P; Huie, R. E.; Ross, A. B. Rate Constants for Reactions of Peroxyl Radicals in Fluid Solutions. *Journal of Physical and Chemical Reference Data* **1990**, *19* (413). https://doi.org/10.1063/1.555854.
(62) Ervens, B.; Volkamer, R. Glyoxal Processing by Aerosol Multiphase Chemistry: Towards a Kinetic Modeling Framework of Secondary Organic Aerosol Formation in Aqueous Particles. *Atmos. Chem. Phys.* **2010**, *10* (17), 8219–8244. https://doi.org/10.5194/acp-10-8219-2010.
(63) Birdsall, A. W.; Hensley, J. C.; Kotowitz, P. S.; Huisman, A. J.; Keutsch, F. N. Single-Particle Experiments Measuring Humidity and Inorganic Salt Effects on Gas-Particle Partitioning of Butenedial. **2019**. https://doi.org/10.5194/acp-2019-423.
(64) Hayyan, M.; Hashim, M. A.; AlNashef, I. M. Superoxide Ion: Generation and Chemical Implications. *Chem. Rev.* **2016**, *116* (5), 3029–3085. https://doi.org/10.1021/acs.chemrev.5b00407.
(65) Castellanos, M. M.; Reyman, D.; Sieiro, C.; Calle, P. ESR-Spin Trapping Study on the Sonochemistry of Liquids in the Presence of Oxygen. Evidence for the Superoxide Radical Anion Formation. *Ultrasonics Sonochemistry* **2001**, *8* (1), 17–22. https://doi.org/10.1016/S1350-4177(99)00047-4.

(66) Wirz, J. Kinetic Studies of Keto–Enol and Other Tautomeric Equilibria by Flash Photolysis. In *Advances in Physical Organic Chemistry*; Elsevier, 2010; Vol. 44, pp 325–356. https://doi.org/10.1016/S0065-3160(08)44006-6.
(67) Bielski, B. H. J.; Allen, A. O. Mechanism of the Disproportionation of Superoxide Radicals. *J. Phys. Chem.* **1977**, *81* (11), 1048–1050. https://doi.org/10.1021/j100526a005.
(68) Garza, A. J. Solvation Entropy Made Simple. *Journal of Chemical Theory and Computation* **2019**, *15*, 3204–3214. https://doi.org/10.1021/acs.jctc.9b00214.